https://doi.org/10.5194/egusphere-2024-1899
Preprint. Discussion started: 15 July 2024

Urban ozone formation and sensitivities to volatile chemical products, cooking emissions, and NO_x across the Los Angeles Basin

Chelsea E. Stockwell[1]*, Matthew M. Coggon[1], Rebecca H. Schwantes[1], Colin Harkins[1,2], Bert Verreyken[1,a,b], Congmeng Lyu[1,2], Qindan Zhu[1,2,c], Lu Xu[1,2,d], Jessica B. Gilman[1], Aaron Lamplugh[1,2,e], Jeff Peischl[1,2,f], Michael A. Robinson[1,2], Patrick R. Veres[1,g], Meng Li[1,2], Andrew W. Rollins[1], Kristen Zuraski[1,2], Sunil Baidar[1,2], Shang Liu[3], Toshihiro Kuwayama[4], Steven S. Brown[1], Brian C. McDonald[1], Carsten Warneke[1]

[1] NOAA Chemical Sciences Laboratory, Boulder, CO, 80305, USA
[2] Cooperative Institute for Research in Environmental Sciences, University of Colorado Boulder, Boulder, CO, 80309, USA
[3] Department of Civil and Environmental Engineering, Northeastern University, Boston, MA, 02115, USA
[4] California Air Resources Board, Sacramento CA USA
[a] now at: Royal Belgian Institute for Space Aeronomy (BIRA-IASB), Brussels, Belgium
[b] now at: Biosystems Dynamics and Exchanges (BIODYNE), Gembloux Agro-Bio Tech, University of Liege, Liege, Belgium
[c] now at: Department of Earth, Atmospheric and Planetary Sciences, Massachusetts Institute of Technology, Cambridge, MA, United States
[d] now at: Department of Energy, Environmental and Chemical Engineering, Washington University in St. Louis, Missouri, USA
[e] now at: Technical Services Program, Air Pollution Control Division, Colorado Department of Public Health and Environment, Denver, CO USA
[f] now at: NOAA Global Monitoring Laboratory, Boulder, CO, 80305, USA
[g] now at: National Center for Atmospheric Research, Boulder, Colorado, USA

Correspondence to: Chelsea Stockwell (Chelsea.Stockwell@noaa.gov)

Abstract. Volatile chemical products (VCPs) and other non-traditional anthropogenic sources, such as cooking, contribute substantially to the volatile organic compound (VOC) budget in urban areas. The impact of these emissions on ozone formation and urban atmospheric chemistry is uncertain. This study employs detailed Lagrangian box modeling and sensitivity analyses to evaluate ozone response to sector-specific VOC and nitrogen oxide (NO_x) emissions in the Los Angeles (LA) Basin during the summer of 2021. The model simulated the photochemical processing and transport of temporally and spatially gridded emissions from the FIVE-VCP-NEI17NRT inventory and accurately simulates the variability and magnitude of O_3 (hourly normalized mean bias = -0.03; R^2 = 0.83), NO_x, and speciated VOCs measured at a ground site in Pasadena, CA. VOC sensitivity analyses show that anthropogenic VOCs (AVOC) enhance daily maximum 8-hour average ozone in Pasadena by 12 ppb, whereas biogenic VOCs (BVOCs) contribute 8 ppb. Of the ozone influenced by AVOCs, VCPs represent the largest fraction at 44% while cooking and fossil fuel VOCs are comparable at 28% each. This study is the first to quantify the contribution of cooking emissions to urban ozone. NO_x sensitivity analyses along trajectory paths indicate the photochemical regime of ozone varies spatially and temporally. The modeled ozone response is primarily NO_x–saturated across the dense urban core and during peak ozone production in Pasadena, but transitions back to NO_x–limited chemistry briefly during late afternoon hours. Lowering the inventory emissions of NO_x by 25% moves Pasadena to NO_x–limited chemistry throughout the majority of the day and shrinks the spatial extent of NO_x–saturation towards downtown LA. Further sensitivity analyses show that using VOCs represented by a separate state inventory requires steeper NO_x reductions to transition to NO_x–sensitivity, further suggesting that accurately representing VOC reactivity in inventories is critical to determine the effectiveness of future NO_x–reduction policies.

1 Introduction

Decreases in emissions of volatile organic compounds (VOCs) and nitrogen oxides (NO_x=NO+NO_2) have coincided with reduced ozone (O_3) pollution in many United States (U.S.) urban centers (Warneke et al., 2012; Jiang et al., 2018; Kim et al., 2022). As reductions from automotive emissions continue, the relative contribution from understudied anthropogenic VOCs (AVOCs), including volatile chemical products (VCPs), to the total emitted VOCs in urban areas continues to rise (McDonald et al., 2018; Gkatzelis et al., 2021b) and is important for O_3 and acetyl peroxynitrate (PAN) formation (Coggon et al., 2021). Other non-traditional emission sources, including commercial and residential cooking, contribute to the urban VOC (Coggon et al., 2024a; Peng et al., 2022; Wernis et al., 2022) and aerosol (Hayes et al., 2013; Robinson et al., 2006; Robinson et al., 2018) mixture, though the atmospheric impacts and spatial/temporal distributions are not well studied. Attributing O_3 to specific VOC emission sources is challenging and some methods rely on reactivity estimates (e.g., maximum incremental activity) to predict O_3 formation potential (OFP), which may not reflect realistic atmospheric processing (Gu et al., 2021a; Venecek et al., 2018). Box models using inventory emissions are a useful tool for O_3 source attribution as they simulate transport and photochemical processing (Abdi-Oskouei et al., 2022; Coggon et al., 2021), while simultaneously enabling sensitivity analyses that directly relate to potential emissions scenarios.

Ozone formation depends on the initial mix and reactivity of VOCs and total NO_x and is known to respond non-linearly to changes in their atmospheric concentrations (Seinfeld, 1989; Kleinman et al., 1997; Kleinman, 2005; Edwards et al., 2014). In regions characterized by high VOC mixing ratios and lower NO_x, O_3 increases with the addition of NO_x since the rate of radical propagation and NO_2 production is limited by NO. This chemical regime is often termed "NO_x–limited" or "NO_x–sensitive". In contrast, if NO_x mixing ratios are high relative to VOC reactivity, the opposite dependence on NO_x is observed and O_3 production is considered "NO_x–saturated" (also termed "VOC–limited", "VOC–sensitive", or "radical–limited"). In this regime, increasing NO_x suppresses OH radicals and limits the production of peroxy radicals, which propagate ozone by reacting with NO to form NO_2. The addition of VOCs or reduction of NO_x in this chemical regime increases O_3 production. Defining these two distinct chemical regimes in urban areas is critical to understanding effective mitigation strategies, and this paper investigates the sensitivity of ozone mixing ratios to changes in emissions and ozone precursors.

The Los Angeles (LA) Basin in California is among the few remaining regions of the U.S. where O_3 mixing ratios exceed the National Ambient Air Quality Standards (NAAQS) for ground-level O_3 (8 h average of 70 ppb) with an extreme classification. Significant efforts to mitigate O_3 production in the LA Basin have focused on emissions control. Reductions in AVOCs, carbon monoxide (CO), and NO_x, primarily from the transportation sector, have reduced ground-level O_3 and particulate matter ($PM_{2.5}$) for decades (McDonald et al., 2018; Warneke et al., 2012; McDonald et al., 2013; Pollack et al., 2013). Many of these downward trends have leveled in recent years, with daily maximum O_3 in some locations actually increasing since 2010 (Jin et al., 2008; Gaudel et al., 2020; Kim et al., 2022). This could be the result of unanticipated trends in emissions (Jiang et al., 2018; McDonald et al., 2018), increasing influence of regional background sources (Silvern et al., 2019), long-range transport (Cooper et al., 2015), changes in atmospheric chemistry (Laughner and Cohen, 2019), and/or consequences of a changing climate with more frequent, longer-lasting, and more intense heatwaves in the U.S. (Habeeb et al., 2015). A clear understanding of O_3 precursors from anthropogenic and biogenic emission sources is key to identifying and targeting NO_x and VOC control strategies in the LA Basin and other major U.S. cities.

The spatiotemporal distribution of emissions and geography of the LA Basin complicate the NO_x dependence of O_3 production, encompassing both NO_x–limited and NO_x–saturated regimes that are seasonally and spatially dependent. Historically, ozone production in the urban core is NO_x–saturated during peak production (Pollack et al., 2012), whereas locations further downwind transition to NO_x–limited chemistry (Jin et al., 2020; Perdigones et al., 2022; LaFranchi et al., 2011; Pusede and Cohen, 2012). The emission reductions prompted by the COVID-19 pandemic showed mixed results across the LA Basin (Parker et al., 2020; Parker et al., 2022; Schroeder et al., 2022; Pennington et al., 2023); however, when considering meteorology, O_3 formation remains NO_x–saturated in the densely populated areas and becomes NO_x–limited further east (Parker et al., 2022) or on average basin-wide (Schroeder et al., 2022). In general, the extent of the NO_x–saturated regime continues to shrink in many urban areas (Koplitz et al., 2022), but spatial O_3 sensitives depend on local and upwind emissions, chemical processing, meteorology, and temperature that can vary throughout the day (Nussbaumer and Cohen, 2020).

Determining the O_3 chemical regime, either directly or indirectly, remains challenging. Studies have evaluated changes to O_3 between weekday to weekend to infer O_3 responses to changes in transportation emissions (termed the "weekday-weekend", or WD–WE, effect). The WD–WE effect centers on lower NO_x on weekends as commercial transportation declines, while VOC emissions remain similar. WD–WE estimates are limited spatially and temporally and are complicated by reduced overnight O_3 titration impacting O_3 background (Peischl et al., 2023). Other approaches estimate changes in VOCs and NO_x through proxies such as satellite column-integrated formaldehyde (HCHO) to NO_2 ratios, which may fail near transitional regimes and are limited by the satellite spatiotemporal resolution (Schroeder et al., 2017). Direct chemical indicators using termination products of HO_x–NO_x cycling (Sillman, 1995; Martin et al., 2004; Vermeuel et al., 2019) or measured/simulated radical production and loss have also been explored (Kleinman et al., 1997; Mao et al., 2010; Abdi-Oskouei et al., 2022; Sakamoto et al., 2019; Robinson et al., 2021). Ozone response to NO_x and VOC perturbations in smog-chambers is the most direct method to evaluate O_3 sensitivity (Wu et al., 2022); however, the approach is practically limited by the location and time of sampling and does not account for dilution, mixing, or deposition (Wu et al., 2024).

Chemical transport models (CTMs) and box models have been used to evaluate the O_3 response to changes in precursor emissions and meteorology. Box models require observational constraints to accurately simulate O_3 mixing ratios, while CTMs require substantial computation time to determine the O_3 response to perturbations. In this study, we employ a multi-process Lagrangian box model that simulates the spatial and temporal evolution of emissions in the LA Basin. This model is used to simulate summertime O_3 formation and to evaluate O_3 sensitivities to changing NO_x and VOCs as air masses transit to two locations downwind of downtown Los Angeles: Pasadena and Redlands, CA. To fully represent the processes that impact O_3 production, the model is informed with anthropogenic and biogenic VOCs from state-of-the-science emissions inventories and employs refined chemical mechanisms, ground-site observations, and meteorological variables from chemical transport models to fully represent the processes that impact O_3 production. The model is first evaluated by comparing it to measurements in Pasadena, CA, collected in the summer of 2021. Then, anthropogenic ozone is attributed to sector-specific VOC sources and the impact of NO_x and VOC perturbations on O_3 formation is quantified to determine the photochemical regime at different locations and times across the LA Basin. Lastly, the O_3 response to total VOCs and their reactivity is evaluated by scaling VOCs to match a separate state emissions inventory.

2 Methods

2.1 Campaign description

The 2021 Southwest Urban NO_x and VOC Experiment (SUNVEx, https://csl.noaa.gov/projects/sunvex/) field campaign was conducted at the California Institute of Technology in Pasadena, CA (34.1403° N, 118.1254° W) from 2 August and 6 September 2021. The site has been previously described as a receptor for the pollutants of downtown Los Angeles and other upwind sources (de Gouw et al., 2018; Ryerson et al., 2013). Measurements were conducted either in a trailer or within a stationary mobile laboratory (34.1403° N, 118.1254° W), both of which sampled air from the same 10 m tower. The mobile laboratory was deployed to characterize the spatial distribution and to determine the local sources of emissions during two time periods (2–6 August; 31 August – 3 September 2021). Times when the mobile laboratory was away from the ground site were excluded from this analysis. Companion measurements were collected nearby at the Ronald and Maxine Linde Laboratory (34.1364° N, 118.1268° W). Table 1 highlights the comprehensive measurements used in this work. Many of these measurements and techniques are described in detail elsewhere (see references in Table 1) and were used to evaluate box model simulations of speciated VOCs, CO, NO, NO_2, total oxidized nitrogen ($NO_y = NO_x + NO_x$ reservoirs), acyl peroxynitrates (PANs), nitric acid (HNO_3), and O_3 (see Sect. 3).

Hourly measurements of O_3 and relative humidity at the Dearborn Reservoir (34.059° N, -117.1473° W) air monitoring site, managed by the South Coast Air Quality Management District (SCAQMD), were used to evaluate the modeled O_3 in Redlands, CA. This site was not equipped extensively, therefore model constraints and evaluations are limited.

Table 1. Summary of instrumentation, utilized measurements, and time resolution reported for the SUNVEx campaign in Pasadena, CA.

Instrument Technique (Abbreviation)	Utilized Measurements	Time Resolution	References
Proton-transfer reaction high-resolution time-of-flight mass spectrometry (NOAA PTR-ToF-MS)	Isoprene, Benzene, Toluene, PCBTF, Methanol, Ethanol, Monoterpenes, Acetone, Octanal, Nonanal, Acetaldehyde, D5-Siloxane	1 Hz	(Yuan et al., 2017)
In-situ gas chromatography mass spectrometry (NOAA GC-MS)	Methyl Ethyl Ketone, Methyl Vinyl Ketone, Methacrolein, Ethane, Ethene, Acetylene	20 min	(Lerner et al., 2017)
Iodide ion chemical ionization time-of-flight mass spectrometry (NOAA Iodide CIMS)	HONO, HNO_3, N_2O_5, organic nitrates, PANs	1 Hz	(Robinson et al., 2022)
Nitrogen Oxides by Cavity Ring Down Spectroscopy (NOAA NOxCaRD)	NO, NO_2, NO_y, O_3	1 Hz	(Wild et al., 2014)
Laser Induced Fluorescence Spectroscopy (NOAA NO-LIF)	NO, NO_2	1 Hz	(Rollins et al., 2020)
Los Gatos Research infrared laser off-axis integrated-cavity-output spectrometer (NOAA LGR)	CO	1 Hz	(Eilerman et al., 2016)
Leosphere 200S Doppler Lidar Dalek 01 (NOAA LIDAR)	Planetary Boundary Layer Height	15 min	(Bonin et al., 2018)
Airmar Wx200 (NOAA MET)	Temperature, Pressure, Relative Humidity	1 Hz	
Teledyne T400, T200U (CIT AQS)	O_3, NO_y	1 min	
Picarro G2307 (CARB HCHO)	HCHO	1 Hz	(Wu et al., 2024)
Filter Radiometry (NOAA jNO2)	jNO_2 photolysis rates	1 Hz	

2.2 Box model configuration

A Lagrangian box model was built using the Framework for 0–D Atmospheric Modeling (F0AM) (Wolfe et al., 2016) and simulates the evolution of emissions, chemistry, and dilution of VOCs, NO_x, CO, and other trace gases as air is transported through the LA Basin. For all species, the box model assumes that mixing ratios are controlled by emissions, chemical reactions, and dilution from vertical expansion with background air, and generally ignores deposition and aerosol uptake. The basic equation describing this evolution of a given species is provided by Eq. (1):

$$\frac{dC_i}{dt} = \frac{E_i(t)}{h(t)\cdot A} + \sum r_i(t) - k_{dil}(t)(C_i - C_{b,i}) \quad (1)$$

where C_i is the concentration of a given species per volume (molec cm^{-3}), $E_i(t)$ is the emission rate based on the time-varying emissions inventory (molec s^{-1}, see Sect. 2.2.2), h(t) is the time-varying planetary boundary layer height from Doppler Lidar measurements or 3D-model retrievals (cm, see Sect. 2.2.4), A is the footprint area represented by the box model (cm^2), $r_i(t)$ are the reaction rates (molec cm^{-3} s^{-1}) that account for the chemical production and loss of C_i, $k_{dil}(t)$ is the time-varying first-order dilution rate calculated based on boundary layer expansion (s^{-1}, see Sect. 2.2.4), and $C_{b,i}$ is the background concentration of a given species mixed from outside of the model.

The model was used to simulate air quality in the LA Basin from 7 August – 7 September 2021. In its basic form, air originates at a specific location determined from back-trajectory analyses (see Section 2.2.1), and is transported over multiple hours through the LA Basin to either the Pasadena or Redlands ground sites. The typical transport in the LA Basin is that of sea breeze meteorology, where air parcels originate near the coast (Santa Monica and San Pedro Bays) and advect inland towards Pasadena, CA over 3–5 h (Washenfelder et al., 2011; Wagner et al., 2012; Hayes et al., 2015). Variability in meteorology and advection can complicate this typical transport pattern; therefore, back-trajectories were calculated to estimate parcel paths across the LA Basin (see Sect. 2.2.1) ending at either the Pasadena or Redlands ground sites (see Fig. 1).

The initial mixing ratios are set to those estimated or measured at the LA coastline. At every 15 minutes (the time interval of the back-trajectory analysis and box model time steps), emissions (E_i) encompassed by the area of the box are mixed into a volume defined by the height of the planetary boundary layer (h) measured by Doppler Lidar and the area footprint of Pasadena (A, equal to 8 × 8 km). The planetary boundary layer evolves as a function of time (t) as the box advects northeastward and is constrained by observations and 3D-model estimates. Due to this expansion, air from the residual layer or free troposphere is entrained into the box using background mixing ratios (see Sect. 2.2.4). This dilution is represented by a first-order rate constant (k_{dil}) and is calculated based on the changes in boundary layer height between model steps. Chemical processing occurs within each model step, and the subsequent outputs inform the initial conditions at the next 15-minute interval. The following sections provide more details describing each process represented by Eq. (1).

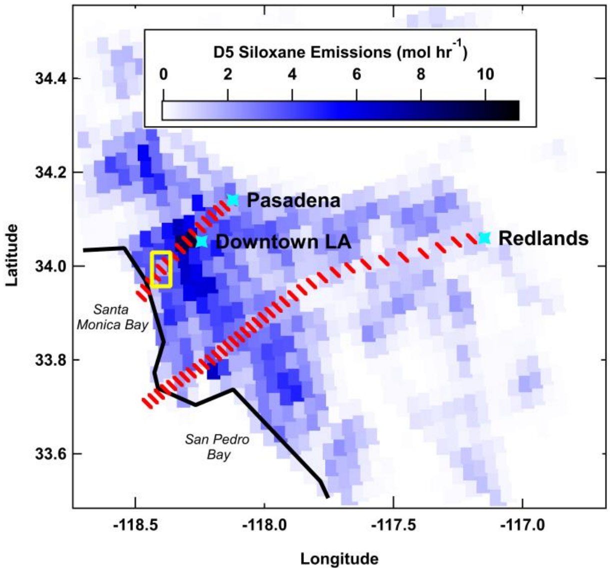

Figure 1: Example FLEXPART back-trajectory paths initiated in Pasadena or Redlands, CA. Red dashes indicate the particle cluster center-of-mass location at 15-minute intervals overlaid with 4 km spatial grids colored by hourly D5-siloxane emission rates extracted from the FIVE-VCP-NEI17NRT inventory. An example model area boundary (8 × 8 km perimeter) used to extract emissions for a single model step is shown in yellow.

2.2.1 FLEXPART-WRF back-trajectory analysis

Trajectory paths were generated with a limited area version of the FLEXible PARTicle dispersion model (FLEXPART) (Stohl et al., 2005) driven with meteorological input provided by the Weather Research and Forecasting v4.2.2 (WRF) numerical weather prediction model (FLEXPART-WRF) (Brioude et al., 2013), and an adapted turbulent parameterization (Verreyken et al., 2019). The dynamical setup from the WRF-Chem model was optimized for the SUNVEx campaign by Verreyken et al. (2024). The model was run on a 4 × 4 km domain covering California and Nevada with the High Resolution Rapid Refresh (HRRR) (Benjamin et al., 2016) model providing initial and boundary conditions. The boundary layer was simulated using the Mellor–Yamada–Nakanishi–Niino (MYNN) (Nakanishi and Niino, 2009) algorithm with the Eddy Diffusivity Mass Flux parameterization (EDMF) (Olson et al., 2019). The model calculates backwards to simulate the trajectory of air parcels to the measurement site near the surface. For air masses initialized every hour in FLEXPART-WRF, trajectories were followed back for 18 hours at 15-minute intervals. The parcel locations were derived as the center-of-mass from the main particle cluster outputted directly by FLEXPART-WRF. Ancillary information used in the F0AM simulation (e.g., photolysis rates, boundary layer height) was obtained from 4–D interpolation along the trajectory from the WRF model coupled with chemistry (WRF-Chem) (Grell et al., 2005) completed for SUNVEx campaign period (Zhu et al., 2024a). More information about the WRF-Chem setup can be found in Zhu et al. (2024a).

The FLEXPART-WRF trajectory analysis generated 744 air mass tracks arriving in Pasadena and Redlands each, every hour from 7 August – 7 September UTC. For comparisons with ground-site observations VOC measurements were excluded when the mobile laboratory conducted drives (31 August – 3 September). Measurements show that winds both at the surface and aloft shift during boundary layer transitions and with temperature fluctuations (Strobach et al., 2024). The FLEXPART analysis captured these fluctuations in meteorology, and trajectory paths reflect this variability. Meteorology was most consistent mid-day when the boundary layer was fully developed and sea-breeze meteorology pushed air masses from the coastline northeastward toward Pasadena as represented in Fig. 1. The back-trajectory analysis revealed that air parcels arriving in Pasadena midday (between 13–18 PDT) transported on average 4–5 h from the coast. The transport further east towards Redlands, CA is more complex, and the back-trajectory analysis suggests air parcels often originated further south and not always along the coastline as represented by Fig. 1.

2.2.2 Emissions

Anthropogenic emissions of CO, NO_x, and VOCs were injected into each model step along the trajectory path from the spatially resolved (4 × 4 km), hourly FIVE-VCP-NEI17NRT emissions inventory (McDonald et al., 2018; He et al., 2024) for the conterminous U.S., extracted for the month of August 2021. Briefly, on-road and non-road engine sources are from the Fuel-Based Inventory of Vehicle Emissions (FIVE) and are updated using fuel sales (Harkins et al., 2021; McDonald et al., 2014). Volatile chemical product (VCP) emissions (McDonald et al., 2018) are included and updated using scaling factors calculated from economic activity statistics. Emissions outside of the U.S., such as Mexico and Canada, as well as shipping emissions, are from the Copernicus Atmospheric Monitoring Service (CAMS) (Doumbia et al., 2021). Oil and gas emissions (O&G) are from the Fuel-based Oil and Gas (FOG) inventory (Francoeur et al., 2021). For pollutants where data is available, powerplant emissions are from the Continuous Emissions Monitoring System (CEMS). Point sources and other area source (gridded) emissions not categorized as VCPs include a mix of evaporative sources, industrial processes, and fossil fuel and biomass combusted related emissions and are taken from the U.S. Environmental Protection Agency's (EPA) 2017 National Emissions Inventory (NEI) (https://www.epa.gov/air-emissions-inventories/2017-nationalemissions-inventory-nei-data) and updated with scaling factors calculated from relevant energy and economic metrics. These area and point emissions are grouped with the other fossil fuel sources in this analysis. VCP sectors include cleaning/degreasing agents, personal care products, adhesives, coatings, inks, and pesticides. The fossil fuel sectors comprise diesel exhaust, evaporative gasoline, gasoline exhaust, off-road diesel and gas, commercial marine vessel, powerplant, and fuel-based oil and gas emissions. Inventory emissions are hourly and produced for three representative days of week; weekdays, Saturdays and Sundays. For the purposes of this analysis, point source emissions have been spatially mapped to the same 4 × 4 km grid that the gridded emissions are available on. Further details about the monthly scaling adjustments to generate near real-time (NRT) emissions to account for rapid changes in human activity, as well as other details of the anthropogenic emissions inventory are described by He et al. (2024). Beyond the emissions configuration described by He et al. (2024), updates to the chemical speciation of the VOCs from VCP emissions were made and are described in Zhu et al. (2024a). The NO_x mixing ratios were initialized within the box model with a NO to NO_2 ratio of 0.25. As the box transits across the LA Basin, NO_x emissions are injected into the box then partitioned to NO and NO_2 based on the previous step. The modeled NO to NO_2 ratio closely matched observations (see Sect. 3.2).

Biogenic emissions (mol s^{-1} km^{-2}) were extracted from 4 km spatially and temporally resolved grids retrieved from WRF-Chem model results for biogenic emissions generated using the Biogenic Emission Inventory System (BEIS) v3.14 inventory for the months of August and September, 2021. The inventory included urban vegetation related to urban land cover types and leaf area index. BEIS input emissions parameters for August and September 2021 were run through WRF-Chem for the study period using the same meteorology used for the FLEXPART-WRF back-trajectory. WRF-Chem uses the BEIS input parameters and meteorology to calculate hourly simulated biogenic emissions specific to each day of the study time period, which are then retrieved from their 4 × 4 km grid. Monoterpene emissions were assumed to be 37% limonene, 53% alpha-pinene, and 10% eucalyptol (Van Rooy et al., 2021; Zhu et al., 2024a).

Recently commercial and residential cooking emissions were observed to be important contributors to urban emissions and were estimated to represent as much as 21% of the total anthropogenic VOC emissions in Las Vegas, NV (Coggon et al., 2024a). These emissions include saturated and unsaturated aldehydes (C_3–C_{10}), long-chain fatty acids, monoterpenes, and ethanol. The FIVE-VCP-NEI17NRT inventory was updated to include cooking emissions estimated using source apportionment reported by Coggon et al. (2024a), and was then spatially distributed onto the same 4 × 4 km grid as other anthropogenic emissions using population density and a temporal profile for human activity. All measured C_8 and C_9 saturated aldehydes (octanal and nonanal) were attributed completely to the cooking sector and served as cooking markers. Ethanol is a major VOC in urban areas and it is challenging to fully resolve its mass using apportionment techniques. The ethanol attributed exclusively to cooking was lower than estimated from cooking VOC fluxes from spatially distributed aircraft flux and indoor measurements (Arata et al., 2021; Pfannerstill et al., 2023), and therefore an upper bound was estimated by increasing ethanol to match the median ethanol to nonanal ratio from aircraft fluxes in LA (Zhu et al., 2024b). There remains some uncertainty in how the cooking VOC mixture and emission rate varies between cities, and Coggon et al. (2024a) discuss that Las Vegas, NV (where the cooking emissions estimate per population was determined) is a major entertainment city and that the number of restaurants per capita may be among the highest in the U.S. While the density of cooking emissions might be higher in Las Vegas, the mass spectrum attributed to cooking compared well to a more recent source apportionment analysis in Toronto, ON, Canada (Rivellini et al., 2024).

Total anthropogenic emissions from FIVE-VCP-NEI17NRT are available on an hourly basis. The total emissions of a given species (E_i; molec s^{-1}) in each model step is outlined by Eq. (2). First, individual emission rate cell grids (e_i; molec s^{-1}) whose centers were encompassed within the defined domain area of the box (A) at a given air parcel location (latitude, longitude) and time (t) were summed. The total emission was then divided by the product of the number of summed grid cells (n) and the grid resolution of the inventory (a_{grid}; 4 × 4 km), and then multiplied by the cross-sectional area of the defined box (A; 8 × 8 km). Finally, emission rates were interpolated to a 15 min time-basis and implemented into Eq. (1) as $E_i(t)$. This renormalization technique was tested at different box model grid resolutions to confirm that the total mass was conserved.

$$E_i = \frac{\sum_0^n e_i}{n \times a_{grid}} \times A \qquad (2)$$

2.2.3 Chemistry

Chemical reactions are represented by the RACM2B-VCP mechanism described in detail by Zhu et al. (2024a). Briefly, the mechanism is based on the Berkeley Regional Atmospheric Chemistry Mechanism Version 2 (RACM2_Berkeley2.0) mechanism, which incorporates a more complex representation of organic nitrate chemistry (Zare et al., 2018) along with monoterpene and isoprene oxidation (Browne et al., 2014). Reactions for oxygenated VOCs primarily emitted from VCPs are incorporated based on the reactions described by (Coggon et al., 2021) and include surrogates for alcohols and glycol ethers (isopropanol, propylene glycol, glycerol). Additional reactions for specific VCP tracers of personal care products (D5-siloxane), solvent-borne coatings (parachlorobenzotriflouride, PCBTF), adhesives (D4-siloxane), and insecticides (p-dichlorobenzene) (Gkatzelis et al., 2021a) are included to track VCP tracer emissions and chemistry in the chemical transport models. Additional chemistry for long-chain saturated and unsaturated aldehydes was added to reflect the OH oxidation of key cooking emissions and the varying chemical pathways forming O_3 and PAN production. This included the addition of lumped saturated and unsaturated cooking aldehydes along with explicit reactions for octanal and nonanal (Coggon et al., 2024a). The reaction rates and product branching ratios for the OH and NO_3 oxidation of lumped saturated cooking aldehydes (CALD), nonanal (NALD), and octanal (OALD) are based on calculations from GECKO-A (https://geckoa.lisa.u-pec.fr/index.php)(Aumont et al., 2005), IUPAC (Mellouki et al., 2021), and Atkinson and Arey (2003). The reaction rates and branching ratios for OH, O_3, and NO_3 oxidation of lumped unsaturated cooking aldehydes (CUALD) are assumed to be generally similar to methacrolein oxidation with minor updates to the products to consider that CUALD has 5 carbons. The cooking mechanism updates are outlined in Supp. Table 1. The distribution of the inventory cooking emissions and the VOC OH reactivity chemically lumped to RACM2B-VCP species is shown in Supplemental Fig. S1. The unresolved mass from source apportionment was attributed to hydrocarbons, which typically fragment in the PTR-ToF-MS and have been reported in laboratory cooking studies (Schauer et al., 1999).

The RACM2B-VCP mechanism used in WRF-Chem simulations during SUNVEx (Zhu et al., 2024a) included a parameterization for the aerosol uptake of isoprene nitrates, monoterpene nitrates, and added the uptake of several inorganic species

https://doi.org/10.5194/egusphere-2024-1899
Preprint. Discussion started: 15 July 2024

using uptake coefficients, aerosol surface area, and aerosol diameter. In this work, these mechanisms were reverted back to the constant reaction rates for isoprene and monoterpene nitrates employed by RACM2_Berkeley2.0 as estimated by Zare et al. (2018). Additionally, the aerosol uptakes of NO_3, NO_2, and HO_2 were ignored as aerosol parameters were not extracted from the WRF-Chem runs.

2.2.4 Meteorology, dilution, and entrainment

The model was constrained with meteorological measurements of pressure, temperature, and relative humidity conducted at the ground site. Photolysis frequencies for key chemical species needed in RACM-based mechanisms were retrieved along the trajectory from 4–D interpolation of the WRF-Chem simulation. The Tropospheric Ultraviolet and Visible radiation model version 5.3.2 (Madronich and Flocke, 1997) was used for photolysis parameterization and mapped to RACM2B-VCP as outlined by Zhu et al. (2024a). Photolysis frequencies account for photon attenuation by clouds or highly absorbing aerosol (e.g., biomass burning smoke). To improve photolysis representation in the box model, the WRF-Chem calculated photolysis frequencies were scaled using observed NO_2 photolysis rates at the ground site (jNO_2) ratioed to WRF-modeled jNO_2. This adjustment was not applied overnight when jNO_2 was near zero. Measured jNO_2 was interpolated during periods when shadows blocked instrument retrievals.

An entrainment rate was applied to account for dilution with surrounding air from the expansion of the planetary boundary layer (PBL) between model steps taken from Doppler Lidar measurements. A constant dilution ($0.3\ h^{-1}$) was iteratively determined from a best fit with observations and applied as the boundary layer collapsed from day-into-night to account for some advection and diffusive mixing. In general, Doppler Lidar measured PBL heights were used to estimate entrainment rates, though there were a few trajectories where WRF-Chem simulated PBL led to improved model agreement. The regional background concentrations for most VOCs were negligible compared to primary emissions in the dense urban core. For species with larger backgrounds including small oxygenates, the box was diluted with regional background mixing ratios estimated from mobile laboratory measurements, regional air quality monitoring stations, or from WRF-Chem chemical concentrations retrieved near the coast. Ozone concentrations were initialized using mixing ratios measured at a surface air quality monitoring site near the coast during the day (Westchester SCAQMD; 33.9551° N, 118.4305° W) or fixed to 10 ppb overnight. The background O_3 mixing ratios entrained into the box volume ranged from 20–45 ppb based on typical mixing ratios observed in the free troposphere above Pasadena in 2023 using the Jet Propulsion Laboratory's Small Mobile Ozone Lidar (https://tolnet.larc.nasa.gov/download).

3 Model evaluation

3.1 Ozone

Figure 2A shows the measured and simulated time-series of hourly O_3 in Pasadena during the SUNVEx campaign. The box model accurately predicts O_3 variability with a normalized mean bias (NMB) of -0.03 and a correlation coefficient (R^2) of 0.83. The NMB is taken as the hourly mean of the model (M) relative to the hourly observational mean (O) minus one as shown in Eq. (3).

$$\mathrm{NMB} = \frac{\mathrm{M}}{\mathrm{O}} - 1 \tag{3}$$

The box model is primarily limited during boundary layer and meteorological transitions as surface winds and temperatures shift in the early mornings and late evenings. This is evident as the boundary layer collapses and transitions to stagnant winds overnight, which results in VOCs and NO_x accumulation and subsequent O_3 titration that is not always fully captured in the model (Strobach et al., 2024). The model's ability to recreate O_3 production during daylight hours (7:00–19:00 Local Time, LT) is better on average and yields a NMB of -0.01 with an average absolute bias of -1.0 ppb. A companion 3D chemical transport simulation (WRF-Chem) was configured over the LA Basin during SUNVEx with FIVE-VCP-NEI17NRT emissions and a similar RACM2B-VCP mechanism scheme. The 3D model more explicitly represents complex meteorology and vertical/horizontal transport over broader spatial scales and accurately simulated O_3 in Pasadena and at 11 additional sites across the LA Basin. Zhu et al. (2024a) reported a NMB of +0.08 and a R^2 of 0.83 in Pasadena. While the box model is constrained to simpler meteorological assumptions, the general agreement between these two models provides confidence that the box model can be used to conduct detailed VOC and NO_x sensitivity analyses (further described in Sect. 4) that are computationally too expensive in a 3D model.

The time series in Fig. 2A and diel pattern in Fig. 2B show peak O_3 in Pasadena typically occurred between 13:00 and 15:00 LT, whereas peak O_3 in Redlands occurred between 15:00 and 17:00 LT (Fig. S3B). As indicated in Fig. 2, the model overpredicts O_3 during peak production (NMB = +0.03; absolute bias = +2.1 ppb), which was not obvious from the calculated NMB since the estimate included all daytime hours on the shoulders of peak production. The box model mechanisms primarily include gas-phase

https://doi.org/10.5194/egusphere-2024-1899
Preprint. Discussion started: 15 July 2024

chemistry, which differs from the full 3D-model RACME2B-VCP mechanism used in WRF-Chem. The simplified mechanism used in the box model is missing processes that include HO_2, inorganic, and aerosol loss pathways, but the box model simulation agrees well with the more complex chemical transport model. The day-to-day agreement varies in both models and is likely driven by uncertainty in meteorology, dilution, and vertical distribution.

The FIVE-VCP-NEI17NRT inventory reflects temporal and spatial usage patterns including those that describe differences in emissions on week versus weekend days and heavy-duty vehicle usage impacting NO_x (Yu et al., 2023). The inventory generally does not reproduce VCP and fossil fuel VOC fluctuations driven by temperature that might be expected with evaporative changes. The temperature sensitivity of biogenic VOCs (BVOCs), including isoprene from BEIS, is captured and reflected in the O_3 variability throughout August as shown by Zhu et al. (2024a). While model-measurement comparisons vary day-to-day, on average the model accurately reproduces O_3 during primary production and therefore all trajectories are included in further analysis. The daily maximum 8-hour average (MDA8) O_3 is important when considering the NAAQS set at 70 ppb for ground-level ozone. Supplemental Figure S2 shows the O_3 diel profile for the 8-hour moving average during the sampling period and MDA8 O_3 from the model (60.6 ± 1.9 ppb) compared well with observations (60.4 ± 13.3 ppb) in Pasadena. The modeled O_3 showed some sensitivity to transport time, and therefore the reported MDA8 O_3 is the average ± standard deviation for transport times ranging from 4–5 h.

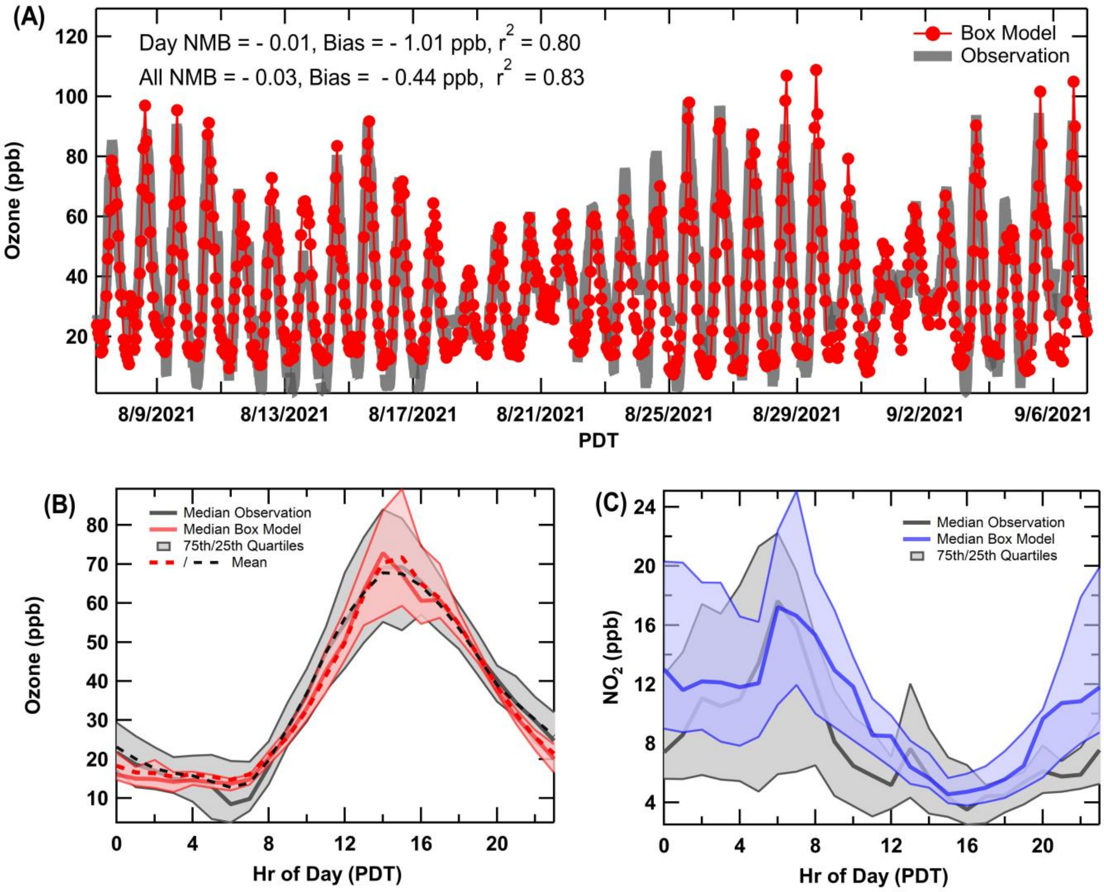

Figure 2: (A) The observed ozone time series (grey lines) overlaid with box model output (red markers) in Pasadena, CA. (B) The median diel profile of modeled (red) and measured (grey) ozone. The mean is a dashed line and the median is marked by the solid line with shaded regions indicating the 75th and 25th quartile ranges. (C) The median diel profile of NO_2 observations (grey) and model output (blue).

The modeled and observed O_3 time series and diel pattern for Redlands, CA is shown in Supplemental Figs. S3A and S3B. The model configuration yields a NMB of -0.01 and an R^2 of 0.67, and while the model effectively reproduces average O_3, the periods of difference are more frequent than in Pasadena, with a larger spread in the 25th and 75th quartile ranges. The NMB and absolute bias during peak production periods (15:00–17:00 LT) were -0.06 and -5 ppb, respectively. The complex meteorology, topography, and uncertain dilution further downwind from the urban core complicate the model's ability to accurately simulate O_3 variability. Additionally, while O_3 is produced from local sources, the transport of O_3, VOCs, and NO_x from upwind sources becomes relatively more important. The population density is lower in the eastern portion of the Basin, but NO_x still accumulates to mixing ratios comparable to downtown LA (Nussbaumer et al., 2023; Chen et al., 2013). The model simulations in Pasadena demonstrate that the emissions and chemistry in the model are accurate, and the main difference in Redlands is that direct measurements of PBL height are not available to constrain dilution, where instead constant dilution rates (0.1–0.2 h^{-1}) were assumed. While the meteorological constraints on the model to Redlands are more limited, the results provide a useful comparison to the Pasadena site for the O_3 sensitivity analyses outlined in Sect. 4.2.

3.2 NO_x and NO_y

Figure 2C shows the modeled and measured NO_2 diel pattern and demonstrates that the relative amounts of daytime NO_2 are captured well by the model. Both the measurements and model exhibit an early morning increase as traffic emissions mix into a shallow boundary layer. The median NO_2 in the model agrees to within measurement uncertainties during peak ozone (13:00–15:00 LT). The diel patterns of NO and NO_x are shown in Supplemental Fig. S4A–B. NO_2 is less variable than NO during the day, though the observations show a small enhancement of NO_2 around 13:00 LT attributed to the transport and arrival of the downtown LA plume (Borbon et al., 2013). The model shows a small, yet discernible enhancement in NO_2 around 12:00 LT. The diel profiles for several longer-lived VOCs, predominately associated with the transportation sector (e.g., benzene and carbon monoxide) show a perceptible mid-day enhancement shifted later in the day around 14:00 LT (see Supplemental Fig. S5). This suggests that the model is capturing the downtown LA plume as expected from previous work (de Gouw et al., 2018), but with a small difference in timing compared to the observations. The observations are likely influenced by local anthropogenic sources since the site was located near parking facilities on a university campus in proximity to other commercial buildings and on-campus traffic. The model configuration yields a NMB during daylight hours of +0.22 for NO_x, with a positive bias in NO_2 and a negative bias in NO (see Fig. S6). The NMB lowers to -0.03 when limiting to afternoon hours when O_3 is primarily enhanced (12:00-16:00 LT). The model allows the ratio of NO to NO_2 to vary and the modeled ratio closely matches observations (Fig. S4C). The diurnal profile of modeled NO_y is shown with the observed NO_y diurnal in Supplemental Fig. S4D. Additional NO_y measurements on top of the Linde Laboratory were higher than those measured at the primary site and the modeled NO_y falls between the two measurements during peak ozone.

3.3 VOCs

Model evaluation of VOCs showed similar results as O_3 and NO_x. Supplemental Figure S6 summarizes the NMB and correlation coefficients (R^2) for observed species that overlap with explicit compounds in the RACM2B-VCP mechanism on an hourly timescale. The NMB calculations are shown for all species during daylight hours when chemistry is important (7:00–19:00 LT) and for the full simulation including high nighttime mixing ratios that might be influenced by local emissions (de Gouw et al., 2018). The chemistry of secondary products is best explained by the model during midday hours when the boundary layer is fully developed and uncertainties due to dilution and dynamic meteorology are reduced. In contrast, primary VOCs undergo chemical oxidation during the daytime that cause lower mixing ratios. Generally, the NMB for most VOCs is within ± 50%. Biases are likely a result of uncertainties in the emissions inventory as well as influences of local emission sources on hourly surface observations. While the model cannot reproduce rapid fluctuations in absolute mixing ratios caused by local sources, it does capture concentration trends across the sampling period as shown in Fig. 3A-D. The time series and median diel patterns for selected VOC tracers show that the model over-accumulates many VOCs at night, even when using enhanced PBL heights prescribed by WRF-Chem. Considering the meteorological limitations of the box model and challenges in both measuring and modeling the nocturnal boundary layer (Lee et al., 2023), the agreement within a factor of two overnight is reasonable. Relatively, daytime agreement is more important to investigate O_3 production chemical regimes as will be discussed in Sect. 4.2. The VOC tracers in Fig. 3A–D were chosen to represent various emission source sectors including toluene for mobile sources, methyl vinyl ketone (MVK) + methacrolein (MACR) for biogenics, D5-siloxane for VCPs, and octanal for cooking. Additional diel patterns for overlap species are compiled in Supplemental Fig. S5.

Aromatic VOCs emitted predominately by the mobile sector (toluene, benzene) are slightly overpredicted during the day, but the diel patterns, especially for benzene (Fig. S5), capture the afternoon enhancement that represents the LA plume. This suggests that the traditional mobile sources are well represented in the emissions inventory. Oxygenated VOCs from VCPs contribute significantly to the urban VOC makeup and reactivity in large cities (Coggon et al., 2021; McDonald et al., 2018) and are represented explicitly in the emissions inventory and the RACM2B-VCP mechanism. This includes the chemistry of several oxygenated VOCs as outlined by Coggon et al. (2021) (methanol, ethanol, isopropanol, ethylene glycol, propylene glycol, glycerol, acetone) and additional VCP tracers added to the mechanism by Zhu et al. (2024a) including D5-siloxane, D4-siloxane, and PCBTF used in personal care products, adhesives, and coatings/paints. These VCP tracers were generally overestimated by the model and similar model-measurement VCP biases were observed when evaluating WRF-Chem simulation with SUNVEx ground site data. It is challenging to evaluate inventories at a single site, and agreement generally improves when averaged across several ground sites or when compared to aircraft observations as shown in Zhu et al. (2024a).

Coggon et al. (2024a) showed that octanal and nonanal are emitted by cooking activities and were added to the model inventory and chemical mechanisms, along with additional saturated and unsaturated aldehydes, fatty acids, monoterpenes, and ethanol based on a VOC source apportionment in Las Vegas, NV. The modeled octanal agrees well with the measurements at night, but is low midday when local lunchtime cooking activity is expected. This suggests better constraints on the temporal variability of cooking VOCs are needed in the inventory. Ethanol has been shown previously to be emitted by cooking activities indoors (Arata et al., 2021), though at higher amounts than was resolved by source apportionment in Las Vegas, NV. The ethanol diel pattern (Fig. S5) from the base scenario agrees well with observations before noon, but remains low in the afternoon to early evening. Additional measurements in urban areas are needed to better constrain the temporal pattern and magnitude of cooking VOCs, including ethanol, in the emissions inventory.

The model using the biogenic inventory BEIS v3.14 underestimated isoprene, MACR, and MVK in Pasadena. Evaluations of BEIS v3.61 with v3.14 suggest leaf canopy and land-use updates increase BVOC emissions across California (Bash et al., 2016). To better account for the influence of biogenic emissions on modeled O_3 production, BEIS v3.14 emissions were increased by 50% to match MACR and MVK, the first-generation oxidative products of isoprene, which have much longer lifetimes compared to isoprene and better represent upwind atmospheric chemistry of emission (Warneke et al., 2010). Even after scaling the biogenic emissions up, both isoprene and monoterpenes remain underpredicted compared to observations. Pasadena is more densely vegetated than many areas upwind in the Basin, and Coggon et al. (2024b) showed that the ground site was significantly impacted by local vegetation. Therefore, it is not unexpected that observations are higher and may not be representative of the entire Basin.

The simulated mixing ratios of secondary products including PAN, nitric acid (HNO_3), formaldehyde (HCHO), and acetaldehyde (CH_3CHO) are biased low, but within 25%. Formaldehyde and acetaldehyde are large contributors to VOC reactivity in urban areas. Both are directly emitted, but are mostly formed by atmospheric chemistry, where major precursors include isoprene and alkenes (Luecken et al., 2012; de Gouw et al., 2018). Acetaldehyde is also important for PAN formation, which itself is an important NO_x and radical reservoir. Lastly, HNO_3 represents a dominant sink of radicals and NO_x. Based on this level of model-measurement agreement, the model adequately represents the important emissions and chemical reactions that influence O_3 formation necessary to perform sensitivity analyses to determine meaningful relationships between VOC emission sectors, NO_x, and the O_3 observed at the Pasadena ground site (Sect. 4).

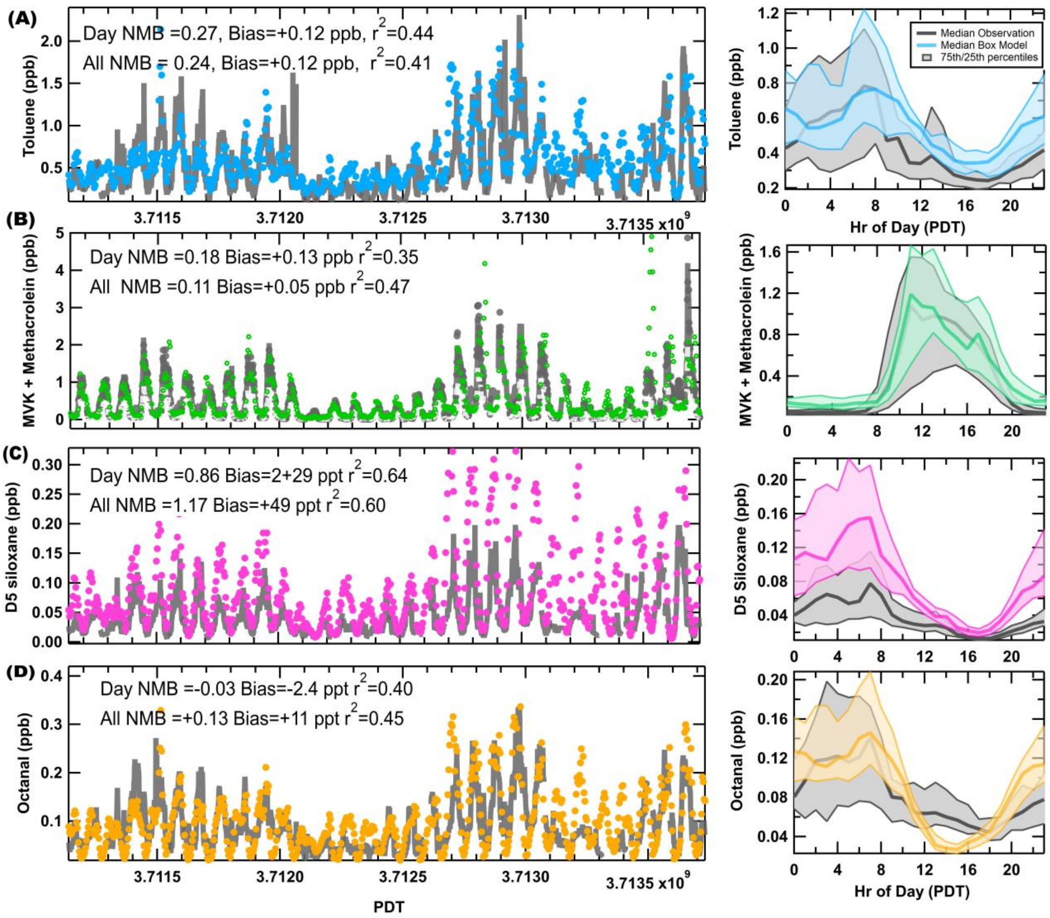

Figure 3: Left Panel: The time-series of box model output concentrations (ppb) overlaid with observations (grey lines) in Pasadena. The selected VOCs include (A) toluene (mobile sources, blue dots), (B) methacrolein plus methyl vinyl ketone (biogenics, green dots), (C) D5-siloxane (VCPs/personal care, pink dots), and (D) octanal (cooking, orange dots). Right Panel: The median diel pattern for each VOC box model output (colored) overlaid with observations (grey). Shaded regions indicate the 75th and 25th quartile ranges.

4 Sensitivity analysis

4.1 Contribution of anthropogenic and biogenic VOCs to ozone

VOC sensitivity analyses were conducted to evaluate the contribution of anthropogenic and biogenic VOCs to the amount of O_3 produced at the Pasadena and Redlands ground sites. For each VOC sensitivity test, emissions for VOCs from an individual emission sector were set to zero ($Sector_i\ VOCs = 0$), while NO_x emissions remained constant, and the change in ozone (ΔO_3) was calculated by comparison to the base case simulation with full emissions. The ozone contribution from each anthropogenic emission sector in the FIVE-VCP-NEI17NRT inventory was summed to estimate the total contribution of anthropogenic VOCs to O_3 (termed “AVOC ozone”) following Eq. (4).

$$AVOC\ Ozone = \sum_{i}^{\#\ of\ sectors} Ozone_{Base\ Case} - Ozone_{Sector_i\ VOCs=0} \tag{4}$$

In order to test for non-linearity in the response of this approach, additional sensitivity analyses were also conducted by reducing individual source sector VOCs by 10% rather than zeroing completely, then multiplying the O_3 change by a factor of 10. The results from both tests agree to within 2% on average for anthropogenic sectors. It is important to note that the anthropogenic O_3 contributions would likely increase for the fossil fuel sectors if both VOCs and NO_x were removed, however, zeroing both

https://doi.org/10.5194/egusphere-2024-1899
Preprint. Discussion started: 15 July 2024

VOCs and NO_x from fossil fuels would significantly alter O_3 chemical regimes. Similar analyses were conducted for the BEIS inventory to determine the contribution of biogenic VOCs to ozone (termed "BVOC ozone"). In Sect. 4.2 we will show that O_3 production in Pasadena occurs at the transition from NO_x–saturated to NO_x–sensitive chemistry; thus, the analyses described below reflects AVOC and BVOC O_3 produced under predominantly NO_x–saturated (i.e. VOC–limited) conditions.

The pie chart in Fig. 4A shows the source sector contributions of AVOC to MDA8 O_3 (total contribution: 12 ppb). The distribution shows that AVOCs from VCP sectors account for 44% of the anthropogenic O_3 while fossil fuels and other area emissions each account for 28%. In contrast, Coggon et al. (2021) showed fossil fuels were 60% of the AVOC O_3 in NYC. The magnitude and spatial distribution of both VCP and fossil fuel emissions differs between the cities, likely driven by differing population and traffic densities. This includes a larger contribution from off-road engines in LA (Kim et al., 2022; Khare and Gentner, 2018). The dominant VCP source sectors in LA were significantly different than in NYC. The construction-related industrial sectors, such as coatings and adhesives, contribute >70% of the VCP O_3 compared to <50% in NYC. Coatings and adhesives emit aromatics and alkanes, where aromatics are more efficient at producing ozone than the most oxygenated VOCs (Carter, 2010) that are dominant ingredients in household and other consumer sources (e.g., personal care products and cleaning agents) (Coggon et al., 2021). Qin et al. (2021) estimated that 9 ± 2 ppb of MDA8 O_3 in LA in the early summer of 2010 was due to VCPs. This is higher than estimated in this work (5.2 ± 0.66 ppb) with a higher relative contribution to the total MDA8 O_3. The absolute MDA8 O_3 likely differed between studies due to the seasonality of biogenic O_3 production, while the absolute VCP VOC contribution differs with usage and regulation changes in the last decade. Seltzer et al. (2022) attributed 4 ppb of midday O_3 (up to 6–8 ppb) to VCPs in Los Angeles using 2016 emission estimates. Coggon et al. (2021) attributed 5–12 ppb O_3 from VCPs downwind of NYC, while Abdi-Oskouei et al. (2022) attributed 2.7 ppb to VCPs in Chicago. Overall, this work agrees with previous assessments of VCP contributions to O_3.

Cooking emissions were not considered in any previous analysis and in Pasadena the contribution to AVOC ozone nearly matches fossil fuels (28%). Primary cooking emissions include a mix of both saturated and unsaturated aldehydes, including dienals, that have a high reactivity towards OH radicals. Supplemental Figure S1B shows these aldehydes account for over 70% of the cooking VOC OH reactivity and therefore it is not surprising that over a quarter of the anthropogenic ozone is attributed to cooking VOCs, which was not recognized as a significant source previously. There remains some uncertainty in the O_3 attribution since studies measuring both the composition and magnitude of cooking emissions in outdoor urban areas are limited (Rivellini et al., 2024; Coggon et al., 2024a). Increasing the source apportioned cooking ethanol to improve agreement with aircraft flux estimates (see Sect. 2.2.2) produces 0.6 ppb more O_3 from cooking emissions, which provides some measure of uncertainty for O_3 attributed to cooking VOCs. This highlights the need for more measurements to refine emissions estimates in urban areas. This is the first study to show the cooking VOC contribution to O_3 formation in urban areas and it is clear that cooking emissions are important for AVOC O_3 formation.

Biogenic emissions are seasonally and temperature dependent (Guenther et al., 1993) and can contribute significantly to VOC reactivity and O_3 formation during summer (Gu et al., 2021b; Liu et al., 2022). It is critical to quantify the impact of urban vegetation and biogenic VOCs on O_3 and air quality as their impact can minimize the effectiveness of VOC emissions control (Schlaerth et al., 2023). The model suggests that BVOC MDA8 O_3 in Pasadena was ~ 8 ppb, or approximately 40% of total VOC MDA8 O_3 (i.e., AVOC + BVOC MDA8 O_3). Figure 4B shows the average sectoral distribution of O_3 as air is transported from the coast and ending at Pasadena at 15:00 LT. This increase in BVOC contribution to O_3 from the coast inland is consistent with a VOC OH reactivity analysis in the South Coast Air Basin (Liu et al., 2022). Along the entire trajectory, BVOCs account for a significant fraction of the total VOC O_3 and is comparable to AVOC ozone. The BVOC fraction of O_3 is an upper bound, since BVOCs prescribed by BEIS were increased by 50% as described in Sect. 3.3. While anthropogenic VOCs significantly decreased over the past decades, urban vegetation and their biogenic VOC emissions generally remain constant and will continue to be a major contributor to urban O_3 formation, especially in NO_x–saturated regimes like downtown LA as will be described below.

The AVOC O_3 distribution from the box model sensitivity analysis in Redlands is consistent with what was shown above for Pasadena (Supplemental Fig. S7A). In Redlands the population density is lower, which might be the reason why the relative O_3 contribution from fossil fuels grows slightly from 28% to 31%. There is only a minor decrease in the contribution of cooking and the BVOC contribution grows slightly (Supplemental Fig. S7B), continuing the increasing BVOC O_3 contribution further inland (Fig. 4B) (Liu et al., 2022). Although the spatial distribution of NO_x and VOCs varies basin-wide, the distribution and magnitude of AVOC and BVOC O_3 do not change significantly.

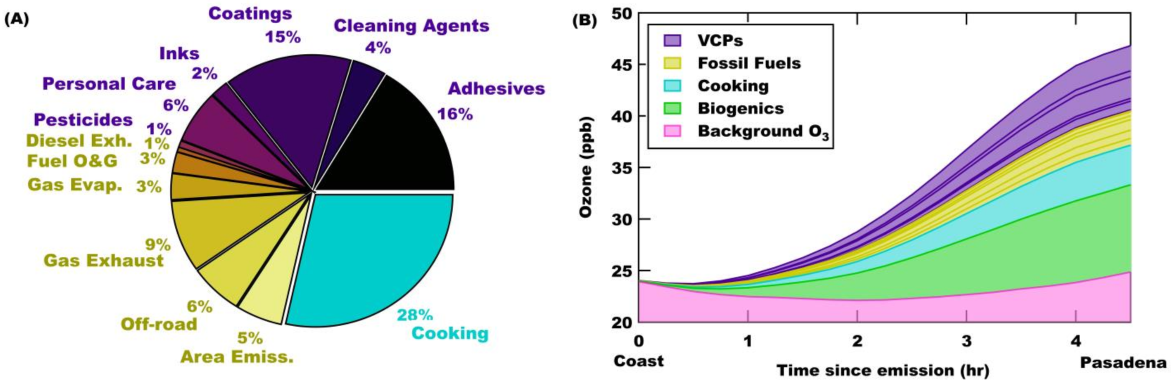

Figure 4: (A) The fractional contribution to MDA8 ozone from anthropogenic VOC sources in Pasadena, CA including: VCPs (purple shading), fossil fuels (yellow shading), and cooking (blue) VOC emissions. (B) The absolute contribution of anthropogenic and biogenic VOC sources to ozone averaged along trajectories initialized near the coast and reaching Pasadena at 15:00 LT.

4.2 Spatial and temporal ozone sensitivity to NO_x

Ozone chemical production regimes are often investigated over broad spatial scales (e.g., the entire contiguous U.S., large urban areas) during seasons with the highest O_3 (Koplitz et al., 2022; Jung et al., 2022; Jin et al., 2020). Studies and methods to investigate seasonal or diurnal trends are more limited (Jin and Holloway, 2015; Wu et al., 2024; Wu et al., 2022). NO_x, VOCs, and meteorology vary widely across the LA Basin, and the Lagrangian trajectory box model is an effective tool to explore ozone responses to NO_x emissions in space and time. Here, O_3 responses to NO_x perturbations are estimated for all of the modeled trajectories. For each trajectory, NO_x emissions were scaled by a factor of 0.2–3 in 10% increments from the base condition while VOCs remained constant. The O_3 response relative to the change in emitted NO_x ($\Delta O_3/\Delta NO_x$) characterizes the chemical regimes as NO_x–limited ($\Delta O_3/\Delta NO_x > 0$), NO_x–saturated ($\Delta O_3/\Delta NO_x < 0$), or transitional ($\Delta O_3/\Delta NO_x = 0$), where the response to NO_x turns over. The initial sign of $\Delta O_3/\Delta NO_x$ identifies the existing chemical regime predicted by the box model at a specific location and time. The difference between the NO_x emissions in the base case simulation to where $\Delta O_3/\Delta NO_x = 0$ approximates the change in NO_x required to transition between chemical regimes. For example, if $\Delta O_3/\Delta NO_x$ at a location and time is initially negative in the base case scenario, lowering NO_x results in a transition from a NO_x–saturated to NO_x–limited regime. The change in NO_x emissions required to reach this transition (termed $\Delta NO_x|_{transition}$) is calculated as:

$$\Delta NO_x|_{transition}(\%) = \frac{NO_x|_{\Delta O3/\Delta NOx=0} - NO_x|_{\text{base}}}{NO_x|_{\text{base}}} \times 100 \qquad (5)$$

where $NO_x|_{\Delta O3/\Delta NOx=0}$ are the NO_x emissions at the transition point and $NO_x|_{\text{base}}$ are those represented by the base case simulation. Hourly trajectories arriving in Pasadena between 12:00 and 20:00 LT are shown in Supplemental Fig. S8, where each location along the trajectory path is colored by $\Delta NO_x|_{transition}$ as a percentage. These trajectories can be used to calculate the average gridded $\Delta NO_x|_{transition}$ between 10:00 and 20:00 LT, which is shown in Fig. 5A. Warmer colors indicate the location is currently NO_x–saturated (negative $\Delta NO_x|_{transition}$), while cooler is NO_x–limited (positive $\Delta NO_x|_{transition}$). At locations over the water or near the coast, where NO_x and VOC emissions are lowest, the regime is NO_x–limited and would require NO_x mixing ratios to increase by more than a factor of 2 to transition to a NO_x–saturated regime. As the air parcels transits across the urban core and through downtown LA, where the density of emissions is high and pollutants increase rapidly, the sensitivity nears the transitional point or crosses into a NO_x–saturated regime. The chemical regime and the amount of NO_x required to transition varies by location and time of day.

Figure 5B shows the average diurnal profile of $\Delta NO_x|_{transition}$ in Pasadena for all trajectories arriving during sunlit hours in August, 2021. The background color highlights when ozone production is NO_x–saturated (red) or NO_x–sensitive (blue). The model suggests that Pasadena is primarily NO_x–saturated for most hours of the day then shifts to NO_x–limited between 15:00 and 18:00 LT. The NO_x diel pattern shown in Supplemental Fig. S4A shows high NO_x availability for reaction with radicals during early daylight hours and then decreases rapidly, allowing radical-radical reactions to compete. Although NO concentrations may be high enough to titrate O_3 during these early hours, this process is unlikely to impact O_3 response during primary production periods. The short period of NO_x–sensitivity would only require a ~10% increase in NO_x emissions to shift back to NO_x–saturated and is later in the afternoon after the period of peak ozone production. Pasadena O_3 production exhibiting NO_x–saturated chemistry, but near the transitional point supports previous modeling conclusions that the NO_x–saturated regime is shrinking in many urban centers, including the LA Basin (Koplitz et al., 2022), and Pasadena is near this transition. This is also supported by previous observations, such as an analysis of the WD–WE effect, where NO_x is lower during weekend days. Ozone trends in Pasadena from the late 2010s show weekend MDA8 O_3 being only marginally higher than weekday averages, whereas the basin-wide averages are the opposite (Kim et al., 2022). Wu et al. (2024) showed clear WD–WE patterns in NO_x emissions in Pasadena with higher median weekend O_3 than weekday concentrations in both August and September, 2021. The results from both of these studies suggest that Pasadena remains NO_x–saturated, though the weekend effect is less pronounced than in earlier decades. In addition, Wu et al. (2024) used direct O_3 response measurements in chamber experiments to show that the O_3 photochemical regime in Pasadena remains NO_x–saturated between 10:00 and 12:00 LT in August, 2021. Uncertainty in the modeled response to NO_x is primarily driven by the absolute NO_x emissions designated by the FIVE-VCP-NEI17NRT inventory. Figure S4 shows that the model tends to overestimate NO_x levels (NMB = + 0.22), although this bias varies in time. Importantly, evaluating model performance using surface observations impacted by local emissions may not be fully representative. Consequently, the inventory NO_x emissions remain unadjusted and are not constrained to match observations. As a result, the subsequent analysis focuses on understanding the O_3 response to inventory NO_x, which is often used to inform emissions control strategies.

Two additional simulations were conducted to evaluate the sensitivity at higher and lower NO_x emission scenarios (Fig. 5B). Increasing the base case NO_x by 25% shows Pasadena sits squarely in the NO_x–saturated regime through the entire day, which represents NO_x levels ~ 4.5 y earlier in 2016–2017 assuming a NO_2 reduction rate estimated from 2011-2015 ($-5.6 \pm 3.6\%\ y^{-1}$) (Jiang et al., 2018). Reducing NO_x by an additional 25% pushes Pasadena into a NO_x–limited regime for over 6 hours of the day during peak O_3. Figure 5B also shows that O_3 production in Redlands was primarily NO_x–limited in August, 2021. This result is consistent with previous modeling observations, which show that air masses in the NO_x–saturated urban core transition to NO_x–limited further downwind of the urban core (Koplitz et al., 2022; Schroeder et al., 2022; Jung et al., 2022). These modeled O_3 responses to NO_x in Redlands compare well to WD–WE evaluations in regions further east in the LA Basin (Kim et al., 2022).

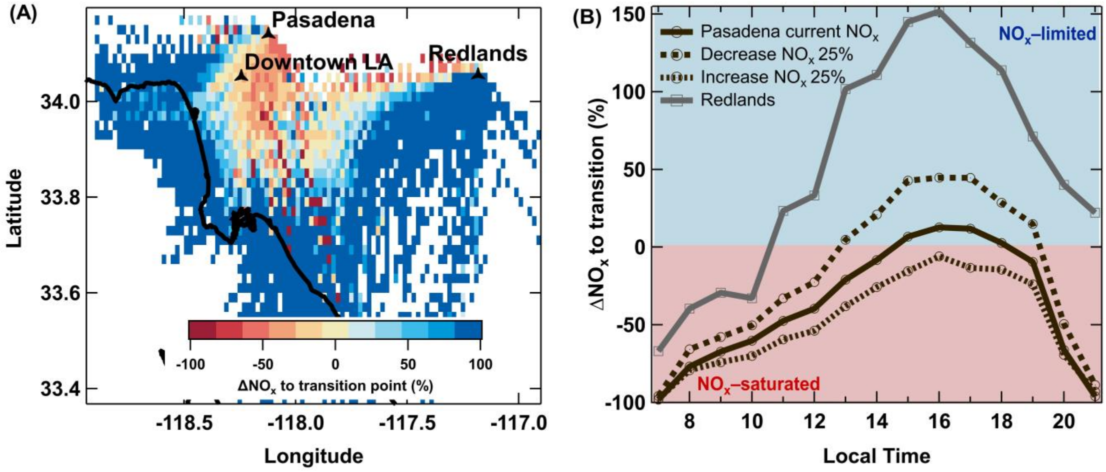

Figure 5: (A) NO_x emissions required to reach the transition between chemical regimes ($\Delta NO_{x|transition}$) averaged in 2 × 2 km grids for locations and times between 10:00 and 20:00 LT (%). Warmer colors (–%) indicate the location is currently NO_x–saturated, while cooler (+%) is NO_x–limited. (B) The predicted average (solid line) change in NO_x needed to transition between photochemical O_3 chemical regimes for the month of August, 2021 in Pasadena, CA. Red shading designates the current chemical regime as NO_x–saturated, blue shading designates NO_x–limited. The dashed lines simulate the sensitivity as the base case NO_x is increased and reduced by 25%. The solid grey line designates sensitivity results in Redlands, CA.

4.3 Impact of inventory selection on O_3 sensitivity

Ozone is also sensitive to total VOCs and their reactivity. Figure 6 shows the baseline average O_3 concentration at peak O_3 (14:00 LT) and its response to changes to NO_x emissions (red line). The vertical hatch marks show the point where O_3 production transitions between chemical regimes ($\Delta O_3/\Delta NO_x \approx 0$) and the dotted line reflects the base-case NO_x emissions. Similar to Fig. 5B, the sensitivity analysis shown in Fig. 6 illustrates that O_3 production in Pasadena is NO_x–saturated at 14:00 LT (negative $\Delta O_3/\Delta NO_x$), and that a ~10% decrease in NO_x would result in a transition to NO_x–sensitive chemistry. These model conditions represent the FIVE-VCP-NEI17NRT emissions described in Sec. 3.3, which includes cooking VOCs and BVOCs from BEIS v3.14 that were increased by 50%.

Figure 6 also compares the FIVE-VCP-NEI17NRT to other inventories, including the National Emissions Inventory (NEI), which is the standard for determining U.S. emissions standards, and the California Emissions Projection Analysis Model (CEPAM2019v1.03) tool used by California Air Resources Board (CARB) to estimate the average annual anthropogenic emissions by region in California. The emissions prescribed by CEPAM2019v1.03 closely match the 2017 NEI inventory (https://ww2.arb.ca.gov/applications/emissions-air-basin). The distributions of VOCs from FIVE-VCP-NEI17NRT and CEPAM2019v1.03 (hereafter designated "CARB CEPAM") are shown in Supplemental Fig. S9 for VCPs, on-road and off-road engines, fuel-based oil and gas, and cooking VOCs in the South Coast Air Basin (SoCAB). In Las Vegas, NV, the fraction of cooking VOCs to the total VOC distribution is less than 1% in the NEI, whereas 21% of the total VOC mass was determined to be cooking-related emissions by source apportionment (Coggon et al., 2024a). The cooking contribution to AVOCs and speciation determined in Las Vegas was distributed in SoCAB based on population density within the FIVE-VCP-NEI17NRT inventory as described in Sect. 2.2.2. To more realistically represent cooking VOCs in the NEI, the O_3 response to NO_x when zeroing cooking emissions is shown as the blue trace in Fig. 6, which shifts Pasadena deeper into NO_x–saturation and lowers peak O_3. Without cooking VOCs, the total VOC reactivity in Pasadena is lower compared to FIVE-VCP-NEI17NRT, and will require a NO_x reduction of approximately 20% to shift into a NO_x–limited photochemical regime. These results show that representing the VOC reactivity from cooking emissions is important for interpreting the impact of NO_x reductions on O_3 formation in Pasadena. Further characterization of cooking VOCs in urban areas and evaluating their representation in models may help inform future O_3 mitigation strategies.

In addition, the VCP emissions from FIVE-VCP-NEI17NRT for 2021 are four times higher than CARB CEPAM for 2017 in SoCAB. This is similar to the study by McDonald et al. (2018), which found that FIVE-VCP VCP emissions in Los Angeles were a factor of 2.5 higher than CARB. Similarly, Qin et al. (2021) showed that scaling the 2011 NEI VCP emissions up by a factor of 3–4, improved agreement with the FIVE-VCP modeled OH reactivity in California. A recent study by Pfannerstill et al. (2023) also identified mismatches in the spatial distribution of VOC emissions within the SoCAB compared to the inventory. While the VOC emissions from on-road engines are comparable, off-road VOCs represented by FIVE-VCP are approximately 50% lower than those in CARB CEPAM. The red trace in Fig. 6 shows the O_3 response to NO_x after scaling FIVE-VCP-NEI17NRT AVOC emissions to reflect what is used in the 2017 CARB CEPAM for VCP, mobile, and cooking sectors. The VOC adjustments lowered total ozone, and suggest even larger model NO_x reductions would be needed to transition to NO_x–limited chemistry in Pasadena (40% decrease needed to reach $\Delta O_3/\Delta NO_x \approx 0$). Finally, the yellow trace shows O_3 responses with unadjusted BEIS v3.14 BVOCs. As expected, lower biogenic emissions push the model further into a NO_x–saturated regime. This sensitivity analysis is used to compare the updated FIVE-VCP-NEI17NRT emissions to anthropogenic and biogenic emissions inventories commonly used in regulatory models.

The sensitivity analyses highlight the impact of the total and the composition of anthropogenic VOCs on O_3 and its response to changing NO_x, especially in a VOC–sensitive regime. Emissions inventories are needed to accurately represent all emission sources and total VOC reactivity (Zhu et al., 2024b) and the uncertainty between inventories leads to uncertainties in the predicted efficacy of emission control strategies. NO_x reductions have been effective in reducing O_3 and it is expected that NO_x reductions will continue in the near future (Schroeder et al., 2022; Kim et al., 2022; Koplitz et al., 2022; Wu et al., 2024; Nussbaumer and Cohen, 2020). Figure 6 demonstrates that with an observationally-constrained inventory (e.g., FIVE-VCP-NEI17NRT), model simulations would suggest that the LA Basin as a whole is nearing a NO_x–sensitive chemical regime and that the spatial extent of NO_x–saturated chemistry is directionally shrinking towards downtown LA. In these model simulations, a 10% decrease in NO_x emissions would result in NO_x–sensitive chemistry in Pasadena during peak O_3 (~14:00 LT). On the other hand, model simulations using emissions representative of the NEI suggest that O_3 production in much of the LA Basin is more NO_x–saturated, and that a nearly 40% decrease in NO_x is needed to transition. These differences are significant and could potentially alter conclusions on the efficacy of NO_x reduction policies. More studies are needed to describe the statistical confidence levels in which various scenarios will achieve a consistent NO_x–limited regime in Pasadena, especially in the context of future O_3 exceedance events that drives O_3 design values. This study demonstrates that accurate VOC representation in models can improve the prediction of O_3 formation, and is required to inform various NO_x and VOC emission reduction decisions to effectively achieve O_3 levels that satisfy the NAAQS.

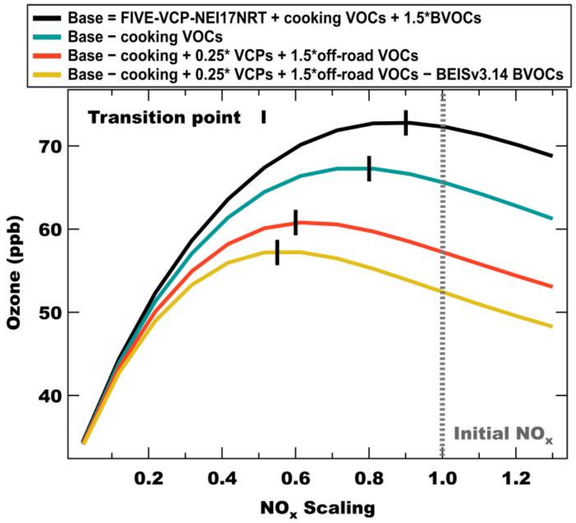

Figure 6: The change in O_3 concentrations averaged at 14:00 LT in Pasadena as NO_x is scaled from its initial mixing ratio (grey dashed line) for the following scenarios: (1) Base model emissions that includes FIVE-VCP-NEI17NRT anthropogenic VOCs, cooking VOCs, and BEIS BVOCs scaled up 50% (black line). (2) Base emissions excluding cooking VOCs (blue). (3) Base emissions excluding cooking VOCs with VCP VOCs scaled down and off-road VOCs adjusted to better match the CARB-CEPAM inventory emissions (red). (4) Scenario 3 with BVOCs scaled down to the original BVOCs prescribed by the BEIS inventory coupled with WRF-Chem (yellow). The location of the transition between photochemical regimes is indicated by the black hatch mark.

5 Conclusions

A detailed, multi-process Lagrangian box model was developed to determine O_3 sensitivities to NO_x and VOC emissions from VCPs, fossil fuels, cooking, and biogenics in the Los Angeles Basin. A comparison of the box model output of O_3, NO_x, and speciated VOCs with measurements in Pasadena, CA during SUNVEx suggests the FIVE-VCP-NEI17NRT gridded inventory is effective in representing LA emissions in space and time. The box model incorporated variables from a 3D-model together with observationally constrained meteorology and updated VOC chemistry to accurately simulate ozone and other products of atmospheric chemistry. This included updated chemical mechanisms that better represent the chemistry of oxygenated VOCs emitted from sources such as VCPs and cooking. The model proved to be a practical tool to evaluate O_3 response to small perturbations and shows that cooking VOCs contribute as much as fossil fuel VOCs to MDA8 O_3 in Pasadena. The relative contributions in other cities likely vary based on restaurant density, VCP usage, and transportation activity, but this remains one of the first studies to show O_3 production from cooking emissions in an urban area. Additional measurements in other cities is critical to evaluate cooking VOC representation in emission inventories, both temporally and spatially. The inclusion of cooking VOCs impacts NO_x and VOC–control assessments, highlighting the importance of accurately representing VOC reactivity and chemistry in inventories and model simulations. The model suggests BVOCs are still an important O_3 precursor that cannot be easily controlled. The modeled ozone sensitivity analysis with full inventory emissions suggest the urban core of Los Angeles including Pasadena is still primarily NO_x–saturated for the majority of the day and shifts to NO_x–limited farther east towards Redlands. Pasadena sits near the transitional point, which suggests that the spatial extent of NO_x–saturation is shrinking across the LA Basin. Scaling FIVE-VCP-NEI17NRT VOC emissions to better reflect emissions represented by the 2017 NEI and CARB CEPAM, lowers absolute O_3 and pushes Pasadena further into NO_x–saturated chemistry. Accurately representing VOCs and their reactivity in emissions inventories is critical to determine absolute O_3 formation, and to determine how NO_x reductions may impact O_3.

Data and code availability

Data for the SUNVEx campaign are available from the NOAA CSL data repository (https://csl.noaa.gov/projects/sunvex/, NOAA Chemical Sciences Laboratory, 2023). WRF-Chem simulations are available at https://github.com/NOAA-CSL/WRF-

Chem_CSL_Publications/tree/main/Qindan_Zhu_et_al_2024 and emissions files from FIVE-VCP-NEI17NRT for the SUNVEx campaign can be found at https://csl.noaa.gov/groups/csl7/measurements/2021sunvex/emissions/

Author Contributions

CES, MMC, LX, JBG, AL, JP, MAR, PRV, AWR, KZ, SB, SL, TK, SB, CW conducted measurements during the SUNVEx and RE-CAP campaigns. CH and ML developed the FIVE-VCP-NEI17NRT inventory with added cooking emissions. BV and CL performed the FLEXPART-WRF analysis. RHS and QZ performed model simulations in WRF-Chem and added cooking mechanisms to RACM2B-VCP. BM oversaw inventory, FLEXPART-WRF, and WRF-Chem development. CES and MMC performed the box model analysis. CES prepared the manuscript with contributions from all co-authors.

Acknowledgements

The O_3 and NO_y measurements on the Caltech campus were supported with funding from the Resnick Sustainability Institute and we thank Paul Wennberg and John Crounse for those measurements and assistance in the campaign organization. We thank J. Andrew Neuman for his assistance with measurements on the Iodide CIMS during SUNVEx. We thank Seyedmorteza Amini for helping configure CARB's mobile research platforms and instrument dataloggers for RECAP-CA, a California-specific companion study to SUNVEx.

Competing interests

The authors have declared that there are no competing interests.

Financial support

This research has been supported by the US Environmental Protection Agency STAR program (grant no. 84001001); Clark County, NV (grant no. 20-022001); the California Air Resources Board (grant no. 20RD002); the Coordinating Research Council (grant no. A-132) and the Cooperative Institute for Research in Environmental Sciences (grant nos. NA17OAR4320101 and NA22OAR4320151)

References

Abdi-Oskouei, M., Roozitalab, B., Stanier, C. O., Christiansen, M., Pfister, G., Pierce, R. B., McDonald, B. C., Adelman, Z., Janseen, M., Dickens, A. F., and Carmichael, G. R.: The Impact of Volatile Chemical Products, Other VOCs, and NOx on Peak Ozone in the Lake Michigan Region, Journal of Geophysical Research: Atmospheres, 127, e2022JD037042, https://doi.org/10.1029/2022JD037042, 2022.

Arata, C., Misztal, P. K., Tian, Y., Lunderberg, D. M., Kristensen, K., Novoselac, A., Vance, M. E., Farmer, D. K., Nazaroff, W. W., and Goldstein, A. H.: Volatile organic compound emissions during HOMEChem, Indoor Air, 31, 2099-2117, 10.1111/ina.12906, 2021.

Atkinson, R. and Arey, J.: Atmospheric Degradation of Volatile Organic Compounds, Chemical Reviews, 103, 4605-4638, 10.1021/cr0206420, 2003.

Aumont, B., Szopa, S., and Madronich, S.: Modelling the evolution of organic carbon during its gas-phase tropospheric oxidation: development of an explicit model based on a self generating approach, Atmos. Chem. Phys., 5, 2497-2517, 10.5194/acp-5-2497-2005, 2005.

Bash, J. O., Baker, K. R., and Beaver, M. R.: Evaluation of improved land use and canopy representation in BEIS v3.61 with biogenic VOC measurements in California, Geosci. Model Dev., 9, 2191-2207, 10.5194/gmd-9-2191-2016, 2016.

Benjamin, S. G., Weygandt, S. S., Brown, J. M., Hu, M., Alexander, C. R., Smirnova, T. G., Olson, J. B., James, E. P., Dowell, D. C., Grell, G. A., Lin, H., Peckham, S. E., Smith, T. L., Moninger, W. R., Kenyon, J. S., and Manikin, G. S.: A North American Hourly Assimilation and Model Forecast Cycle: The Rapid Refresh, Monthly Weather Review, 144, 1669-1694, https://doi.org/10.1175/MWR-D-15-0242.1, 2016.

Bonin, T. A., Carroll, B. J., Hardesty, R. M., Brewer, W. A., Hajny, K., Salmon, O. E., and Shepson, P. B.: Doppler Lidar Observations of the Mixing Height in Indianapolis Using an Automated Composite Fuzzy Logic Approach, Journal of Atmospheric and Oceanic Technology, 35, 473-490, https://doi.org/10.1175/JTECH-D-17-0159.1, 2018.

Borbon, A., Gilman, J. B., Kuster, W. C., Grand, N., Chevaillier, S., Colomb, A., Dolgorouky, C., Gros, V., Lopez, M., Sarda-Esteve, R., Holloway, J., Stutz, J., Petetin, H., McKeen, S., Beekmann, M., Warneke, C., Parrish, D. D., and de Gouw, J. A.: Emission ratios of anthropogenic volatile organic compounds in northern mid-latitude megacities: Observations versus emission inventories in Los Angeles and Paris, Journal of Geophysical Research: Atmospheres, 118, 2041-2057, https://doi.org/10.1002/jgrd.50059, 2013.

Brioude, J., Arnold, D., Stohl, A., Cassiani, M., Morton, D., Seibert, P., Angevine, W., Evan, S., Dingwell, A., Fast, J. D., Easter, R. C., Pisso, I., Burkhart, J., and Wotawa, G.: The Lagrangian particle dispersion model FLEXPART-WRF version 3.1, Geosci. Model Dev., 6, 1889-1904, 10.5194/gmd-6-1889-2013, 2013.

Browne, E. C., Wooldridge, P. J., Min, K. E., and Cohen, R. C.: On the role of monoterpene chemistry in the remote continental boundary layer, Atmos. Chem. Phys., 14, 1225-1238, 10.5194/acp-14-1225-2014, 2014.

Carter, W. P. L.: Development of the SAPRC-07 chemical mechanism, Atmospheric Environment, 44, 5324-5335, https://doi.org/10.1016/j.atmosenv.2010.01.026, 2010.

Chen, D., Li, Q., Stutz, J., Mao, Y., Zhang, L., Pikelnaya, O., Tsai, J. Y., Haman, C., Lefer, B., Rappenglück, B., Alvarez, S. L., Neuman, J. A., Flynn, J., Roberts, J. M., Nowak, J. B., de Gouw, J., Holloway, J., Wagner, N. L., Veres, P., Brown, S. S., Ryerson, T. B., Warneke, C., and Pollack, I. B.: WRF-Chem simulation of NOx and O3 in the L.A. basin during CalNex-2010, Atmospheric Environment, 81, 421-432, 10.1016/j.atmosenv.2013.08.064, 2013.

Coggon, M. M., Stockwell, C. E., Xu, L., Peischl, J., Gilman, J. B., Lamplugh, A., Bowman, H. J., Aikin, K., Harkins, C., Zhu, Q., Schwantes, R. H., He, J., Li, M., Seltzer, K., McDonald, B., and Warneke, C.: Contribution of cooking emissions to the urban volatile organic compounds in Las Vegas, NV, Atmos. Chem. Phys., 24, 4289-4304, 10.5194/acp-24-4289-2024, 2024a.

Coggon, M. M., Stockwell, C. E., Claflin, M. S., Pfannerstill, E. Y., Xu, L., Gilman, J. B., Marcantonio, J., Cao, C., Bates, K., Gkatzelis, G. I., Lamplugh, A., Katz, E. F., Arata, C., Apel, E. C., Hornbrook, R. S., Piel, F., Majluf, F., Blake, D. R., Wisthaler, A., Canagaratna, M., Lerner, B. M., Goldstein, A. H., Mak, J. E., and Warneke, C.: Identifying and correcting interferences to PTR-ToF-MS measurements of isoprene and other urban volatile organic compounds, Atmos. Meas. Tech., 17, 801-825, 10.5194/amt-17-801-2024, 2024b.

Coggon, M. M., Gkatzelis, G. I., McDonald, B. C., Gilman, J. B., Schwantes, R. H., Abuhassan, N., Aikin, K. C., Arend, M. F., Berkoff, T. A., Brown, S. S., Campos, T. L., Dickerson, R. R., Gronoff, G., Hurley, J. F., Isaacman-VanWertz, G., Koss, A. R., Li, M., McKeen, S. A., Moshary, F., Peischl, J., Pospisilova, V., Ren, X., Wilson, A., Wu, Y., Trainer, M., and Warneke, C.: Volatile chemical product emissions enhance ozone and modulate urban chemistry, Proceedings of the National Academy of Sciences, 118, e2026653118, doi:10.1073/pnas.2026653118, 2021.

Cooper, O. R., Langford, A. O., Parrish, D. D., and Fahey, D. W.: Challenges of a lowered U.S. ozone standard, Science, 348, 1096-1097, doi:10.1126/science.aaa5748, 2015.

de Gouw, J. A., Gilman, J. B., Kim, S.-W., Alvarez, S. L., Dusanter, S., Graus, M., Griffith, S. M., Isaacman-VanWertz, G., Kuster, W. C., Lefer, B. L., Lerner, B. M., McDonald, B. C., Rappenglück, B., Roberts, J. M., Stevens, P. S., Stutz, J., Thalman, R., Veres, P. R., Volkamer, R., Warneke, C., Washenfelder, R. A., and Young, C. J.: Chemistry of Volatile Organic Compounds in the Los Angeles Basin: Formation of Oxygenated Compounds and Determination of Emission Ratios, Journal of Geophysical Research: Atmospheres, 123, 2298-2319, https://doi.org/10.1002/2017JD027976, 2018.

Doumbia, T., Granier, C., Elguindi, N., Bouarar, I., Darras, S., Brasseur, G., Gaubert, B., Liu, Y., Shi, X., Stavrakou, T., Tilmes, S., Lacey, F., Deroubaix, A., and Wang, T.: Changes in global air pollutant emissions during the COVID-19 pandemic: a dataset for atmospheric modeling, Earth Syst. Sci. Data, 13, 4191-4206, 10.5194/essd-13-4191-2021, 2021.

Edwards, P. M., Brown, S. S., Roberts, J. M., Ahmadov, R., Banta, R. M., deGouw, J. A., Dubé, W. P., Field, R. A., Flynn, J. H., Gilman, J. B., Graus, M., Helmig, D., Koss, A., Langford, A. O., Lefer, B. L., Lerner, B. M., Li, R., Li, S.-M., McKeen, S. A., Murphy, S. M., Parrish, D. D., Senff, C. J., Soltis, J., Stutz, J., Sweeney, C., Thompson, C. R., Trainer, M. K., Tsai, C., Veres, P. R., Washenfelder, R. A., Warneke, C., Wild, R. J., Young, C. J., Yuan, B., and Zamora, R.: High winter ozone pollution from carbonyl photolysis in an oil and gas basin, Nature, 514, 351-354, 10.1038/nature13767, 2014.

Eilerman, S. J., Peischl, J., Neuman, J. A., Ryerson, T. B., Aikin, K. C., Holloway, M. W., Zondlo, M. A., Golston, L. M., Pan, D., Floerchinger, C., and Herndon, S.: Characterization of Ammonia, Methane, and Nitrous Oxide Emissions from Concentrated Animal Feeding Operations in Northeastern Colorado, Environmental Science & Technology, 50, 10885-10893, 10.1021/acs.est.6b02851, 2016.

Francoeur, C. B., McDonald, B. C., Gilman, J. B., Zarzana, K. J., Dix, B., Brown, S. S., de Gouw, J. A., Frost, G. J., Li, M., McKeen, S. A., Peischl, J., Pollack, I. B., Ryerson, T. B., Thompson, C., Warneke, C., and Trainer, M.: Quantifying Methane and Ozone Precursor Emissions from Oil and Gas Production Regions across the Contiguous US, Environmental Science & Technology, 55, 9129-9139, 10.1021/acs.est.0c07352, 2021.

Gaudel, A., Cooper, O. R., Chang, K. L., Bourgeois, I., Ziemke, J. R., Strode, S. A., Oman, L. D., Sellitto, P., Nédélec, P., Blot, R., Thouret, V., and Granier, C.: Aircraft observations since the 1990s reveal increases of tropospheric ozone at multiple locations across the Northern Hemisphere, Sci Adv, 6, 10.1126/sciadv.aba8272, 2020.

Gkatzelis, G. I., Coggon, M. M., McDonald, B. C., Peischl, J., Aikin, K. C., Gilman, J. B., Trainer, M., and Warneke, C.: Identifying Volatile Chemical Product Tracer Compounds in U.S. Cities, Environmental Science & Technology, 55, 188-199, 10.1021/acs.est.0c05467, 2021a.

Gkatzelis, G. I., Coggon, M. M., McDonald, B. C., Peischl, J., Gilman, J. B., Aikin, K. C., Robinson, M. A., Canonaco, F., Prevot, A. S. H., Trainer, M., and Warneke, C.: Observations Confirm that Volatile Chemical Products Are a Major Source of Petrochemical Emissions in U.S. Cities, Environmental Science & Technology, 55, 4332-4343, 10.1021/acs.est.0c05471, 2021b.

Grell, G. A., Peckham, S. E., Schmitz, R., McKeen, S. A., Frost, G., Skamarock, W. C., and Eder, B.: Fully coupled "online" chemistry within the WRF model, Atmospheric Environment, 39, 6957-6975, https://doi.org/10.1016/j.atmosenv.2005.04.027, 2005.

Gu, S., Guenther, A., and Faiola, C.: Effects of Anthropogenic and Biogenic Volatile Organic Compounds on Los Angeles Air Quality, Environ Sci Technol, 55, 12191-12201, 10.1021/acs.est.1c01481, 2021a.

Gu, S., Guenther, A., and Faiola, C.: Effects of Anthropogenic and Biogenic Volatile Organic Compounds on Los Angeles Air Quality, Environmental Science & Technology, 55, 12191-12201, 10.1021/acs.est.1c01481, 2021b.

Guenther, A. B., Zimmerman, P. R., Harley, P. C., Monson, R. K., and Fall, R.: Isoprene and monoterpene emission rate variability: Model evaluations and sensitivity analyses, Journal of Geophysical Research: Atmospheres, 98, 12609-12617, https://doi.org/10.1029/93JD00527, 1993.

Habeeb, D., Vargo, J., and Stone, B.: Rising heat wave trends in large US cities, Natural Hazards, 76, 1651-1665, 10.1007/s11069-014-1563-z, 2015.

Harkins, C., McDonald, B. C., Henze, D. K., and Wiedinmyer, C.: A fuel-based method for updating mobile source emissions during the COVID-19 pandemic, Environmental Research Letters, 16, 065018, 10.1088/1748-9326/ac0660, 2021.

Hayes, P. L., Carlton, A. G., Baker, K. R., Ahmadov, R., Washenfelder, R. A., Alvarez, S., Rappenglück, B., Gilman, J. B., Kuster, W. C., de Gouw, J. A., Zotter, P., Prévôt, A. S. H., Szidat, S., Kleindienst, T. E., Offenberg, J. H., Ma, P. K., and Jimenez, J. L.: Modeling the formation and aging of secondary organic aerosols in Los Angeles during CalNex 2010, Atmos. Chem. Phys., 15, 5773-5801, 10.5194/acp-15-5773-2015, 2015.

Hayes, P. L., Ortega, A. M., Cubison, M. J., Froyd, K. D., Zhao, Y., Cliff, S. S., Hu, W. W., Toohey, D. W., Flynn, J. H., Lefer, B. L., Grossberg, N., Alvarez, S., Rappenglück, B., Taylor, J. W., Allan, J. D., Holloway, J. S., Gilman, J. B., Kuster, W. C., de Gouw, J. A., Massoli, P., Zhang, X., Liu, J., Weber, R. J., Corrigan, A. L., Russell, L. M., Isaacman, G., Worton, D. R., Kreisberg, N. M., Goldstein, A. H., Thalman, R., Waxman, E. M., Volkamer, R., Lin, Y. H., Surratt, J. D., Kleindienst, T. E., Offenberg, J. H., Dusanter, S., Griffith, S., Stevens, P. S., Brioude, J., Angevine, W. M., and Jimenez, J. L.: Organic aerosol composition and sources in Pasadena, California, during the 2010 CalNex campaign, Journal of Geophysical Research: Atmospheres, 118, 9233-9257, https://doi.org/10.1002/jgrd.50530, 2013.

He, J., Harkins, C., O'Dell, K., Li, M., Francoeur, C., Aikin, K. C., Anenberg, S., Baker, B., Brown, S. S., Coggon, M. M., Frost, G. J., Gilman, J. B., Kondragunta, S., Lamplugh, A., Lyu, C., Moon, Z., Pierce, B. R., Schwantes, R. H., Stockwell, C. E., Warneke, C., Yang, K., Nowlan, C. R., González Abad, G., and McDonald, B. C.: COVID-19 perturbation on US air quality and human health impact assessment, PNAS Nexus, 3, 10.1093/pnasnexus/pgad483, 2024.

Jiang, Z., McDonald, B. C., Worden, H., Worden, J. R., Miyazaki, K., Qu, Z., Henze, D. K., Jones, D. B. A., Arellano, A. F., Fischer, E. V., Zhu, L., and Boersma, K. F.: Unexpected slowdown of US pollutant emission reduction in the past decade, Proceedings of the National Academy of Sciences, 115, 5099-5104, doi:10.1073/pnas.1801191115, 2018.

Jin, L., Tonse, S., Cohan, D. S., Mao, X., Harley, R. A., and Brown, N. J.: Sensitivity Analysis of Ozone Formation and Transport for a Central California Air Pollution Episode, Environmental Science & Technology, 42, 3683-3689, 10.1021/es072069d, 2008.

Jin, X. and Holloway, T.: Spatial and temporal variability of ozone sensitivity over China observed from the Ozone Monitoring Instrument, Journal of Geophysical Research: Atmospheres, 120, 7229-7246, https://doi.org/10.1002/2015JD023250, 2015.

Jin, X., Fiore, A., Boersma, K. F., Smedt, I. D., and Valin, L.: Inferring Changes in Summertime Surface Ozone–NOx–VOC Chemistry over U.S. Urban Areas from Two Decades of Satellite and Ground-Based Observations, Environmental Science & Technology, 54, 6518-6529, 10.1021/acs.est.9b07785, 2020.

Jung, J., Choi, Y., Mousavinezhad, S., Kang, D., Park, J., Pouyaei, A., Ghahremanloo, M., Momeni, M., and Kim, H.: Changes in the ozone chemical regime over the contiguous United States inferred by the inversion of NO(x) and VOC emissions using satellite observation, Atmos Res, 270, 1-14, 10.1016/j.atmosres.2022.106076, 2022.

Khare, P. and Gentner, D. R.: Considering the future of anthropogenic gas-phase organic compound emissions and the increasing influence of non-combustion sources on urban air quality, Atmos. Chem. Phys., 18, 5391-5413, 10.5194/acp-18-5391-2018, 2018.

Kim, S.-W., McDonald, B. C., Seo, S., Kim, K.-M., and Trainer, M.: Understanding the Paths of Surface Ozone Abatement in the Los Angeles Basin, Journal of Geophysical Research: Atmospheres, 127, e2021JD035606, https://doi.org/10.1029/2021JD035606, 2022.

Kleinman, L. I.: The dependence of tropospheric ozone production rate on ozone precursors, Atmospheric Environment, 39, 575-586, https://doi.org/10.1016/j.atmosenv.2004.08.047, 2005.

Kleinman, L. I., Daum, P. H., Lee, J. H., Lee, Y.-N., Nunnermacker, L. J., Springston, S. R., Newman, L., Weinstein-Lloyd, J., and Sillman, S.: Dependence of ozone production on NO and hydrocarbons in the troposphere, Geophysical Research Letters, 24, 2299-2302, https://doi.org/10.1029/97GL02279, 1997.

Koplitz, S., Simon, H., Henderson, B., Liljegren, J., Tonnesen, G., Whitehill, A., and Wells, B.: Changes in Ozone Chemical Sensitivity in the United States from 2007 to 2016, ACS Environmental Au, 2, 206-222, 10.1021/acsenvironau.1c00029, 2022.

LaFranchi, B. W., Goldstein, A. H., and Cohen, R. C.: Observations of the temperature dependent response of ozone to NO_x reductions in the Sacramento, CA urban plume, Atmos. Chem. Phys., 11, 6945-6960, 10.5194/acp-11-6945-2011, 2011.

Laughner, J. L. and Cohen, R. C.: Direct observation of changing NO<i>_x</i> lifetime in North American cities, Science, 366, 723-727, doi:10.1126/science.aax6832, 2019.

Lee, H.-J., Jo, H.-Y., Kim, J.-M., Bak, J., Park, M.-S., Kim, J.-K., Jo, Y.-J., and Kim, C.-H.: Nocturnal Boundary Layer Height Uncertainty in Particulate Matter Simulations during the KORUS-AQ Campaign, Remote Sensing, 15, 300, 2023.

Lerner, B. M., Gilman, J. B., Aikin, K. C., Atlas, E. L., Goldan, P. D., Graus, M., Hendershot, R., Isaacman-VanWertz, G. A., Koss, A., Kuster, W. C., Lueb, R. A., McLaughlin, R. J., Peischl, J., Sueper, D., Ryerson, T. B., Tokarek, T. W., Warneke, C., Yuan, B., and de Gouw, J. A.: An improved, automated whole air sampler and gas chromatography mass spectrometry analysis system for volatile organic compounds in the atmosphere, Atmos. Meas. Tech., 10, 291-313, 10.5194/amt-10-291-2017, 2017.

Liu, S., Barletta, B., Hornbrook, R. S., Fried, A., Peischl, J., Meinardi, S., Coggon, M., Lamplugh, A., Gilman, J. B., Gkatzelis, G. I., Warneke, C., Apel, E. C., Hills, A. J., Bourgeois, I., Walega, J., Weibring, P., Richter, D., Kuwayama, T., FitzGibbon, M., and Blake, D.: Composition and reactivity of volatile organic compounds in the South Coast Air Basin and San Joaquin Valley of California, Atmos. Chem. Phys., 22, 10937-10954, 10.5194/acp-22-10937-2022, 2022.

Luecken, D. J., Hutzell, W. T., Strum, M. L., and Pouliot, G. A.: Regional sources of atmospheric formaldehyde and acetaldehyde, and implications for atmospheric modeling, Atmospheric Environment, 47, 477-490, https://doi.org/10.1016/j.atmosenv.2011.10.005, 2012.

Madronich, S. and Flocke, S.: Theoretical Estimation of Biologically Effective UV Radiation at the Earth's Surface, Solar Ultraviolet Radiation, Berlin, Heidelberg, 1997//, 23-48,

Mao, J., Ren, X., Chen, S., Brune, W. H., Chen, Z., Martinez, M., Harder, H., Lefer, B., Rappenglück, B., Flynn, J., and Leuchner, M.: Atmospheric oxidation capacity in the summer of Houston 2006: Comparison with summer measurements in other metropolitan studies, Atmospheric Environment, 44, 4107-4115, https://doi.org/10.1016/j.atmosenv.2009.01.013, 2010.

Martin, R. V., Fiore, A. M., and Van Donkelaar, A.: Space-based diagnosis of surface ozone sensitivity to anthropogenic emissions, Geophysical Research Letters, 31, https://doi.org/10.1029/2004GL019416, 2004.

McDonald, B. C., Gentner, D. R., Goldstein, A. H., and Harley, R. A.: Long-Term Trends in Motor Vehicle Emissions in U.S. Urban Areas, Environmental Science & Technology, 47, 10022-10031, 10.1021/es401034z, 2013.

McDonald, B. C., McBride, Z. C., Martin, E. W., and Harley, R. A.: High-resolution mapping of motor vehicle carbon dioxide emissions, Journal of Geophysical Research: Atmospheres, 119, 5283-5298, https://doi.org/10.1002/2013JD021219, 2014.

McDonald, B. C., de Gouw, J. A., Gilman, J. B., Jathar, S. H., Akherati, A., Cappa, C. D., Jimenez, J. L., Lee-Taylor, J., Hayes, P. L., McKeen, S. A., Cui, Y. Y., Kim, S.-W., Gentner, D. R., Isaacman-VanWertz, G., Goldstein, A. H., Harley, R. A., Frost, G. J., Roberts, J. M., Ryerson, T. B., and Trainer, M.: Volatile chemical products emerging as largest petrochemical source of urban organic emissions, Science, 359, 760-764, doi:10.1126/science.aaq0524, 2018.

Mellouki, A., Ammann, M., Cox, R. A., Crowley, J. N., Herrmann, H., Jenkin, M. E., McNeill, V. F., Troe, J., and Wallington, T. J.: Evaluated kinetic and photochemical data for atmospheric chemistry: volume VIII – gas-phase reactions of organic species with four, or more, carbon atoms (≥  C4), Atmos. Chem. Phys., 21, 4797-4808, 10.5194/acp-21-4797-2021, 2021.

Nakanishi, M. and Niino, H.: Development of an Improved Turbulence Closure Model for the Atmospheric Boundary Layer, Journal of the Meteorological Society of Japan. Ser. II, 87, 895-912, 10.2151/jmsj.87.895, 2009.

Nussbaumer, C. M. and Cohen, R. C.: The Role of Temperature and NOx in Ozone Trends in the Los Angeles Basin, Environmental Science & Technology, 54, 15652-15659, 10.1021/acs.est.0c04910, 2020.

Nussbaumer, C. M., Place, B. K., Zhu, Q., Pfannerstill, E. Y., Wooldridge, P., Schulze, B. C., Arata, C., Ward, R., Bucholtz, A., Seinfeld, J. H., Goldstein, A. H., and Cohen, R. C.: Measurement report: Airborne measurements of NOx fluxes over Los Angeles during the RECAP-CA 2021 campaign, EGUsphere, 2023, 1-20, 10.5194/egusphere-2023-601, 2023.

Olson, J. B., Kenyon, J. S., Angevine, W. A., Brown, J. M., Pagowski, M., and Sušelj, K.: A Description of the MYNN-EDMF Scheme and the Coupling to Other Components in WRF–ARW, https://doi.org/10.25923/n9wm-be49, 2019.

Parker, H. A., Hasheminassab, S., Crounse, J. D., Roehl, C. M., and Wennberg, P. O.: Impacts of Traffic Reductions Associated With COVID-19 on Southern California Air Quality, Geophys Res Lett, 47, e2020GL090164, 10.1029/2020gl090164, 2020.

Parker, L. K., Johnson, J., Grant, J., Vennam, P., Parikh, R., Chien, C.-J., and Morris, R.: Ozone Trends and the Ability of Models to Reproduce the 2020 Ozone Concentrations in the South Coast Air Basin in Southern California under the COVID-19 Restrictions, Atmosphere, 13, 528, 2022.

Peischl, J., Aikin, K. C., McDonald, B. C., Harkins, C., Middlebrook, A. M., Langford, A. O., Cooper, O. R., Chang, K.-L., and Brown, S. S.: Quantifying anomalies of air pollutants in 9 U.S. cities during 2020 due to COVID-19 lockdowns and wildfires based on decadal trends, Elementa: Science of the Anthropocene, 11, 10.1525/elementa.2023.00029, 2023.

Peng, Y., Mouat, A. P., Hu, Y., Li, M., McDonald, B. C., and Kaiser, J.: Source appointment of volatile organic compounds and evaluation of anthropogenic monoterpene emission estimates in Atlanta, Georgia, Atmospheric Environment, 288, 119324, https://doi.org/10.1016/j.atmosenv.2022.119324, 2022.

Pennington, E. A., Wang, Y., Schulze, B. C., Seltzer, K. M., Yang, J., Zhao, B., Jiang, Z., Shi, H., Venecek, M., Chau, D., Murphy, B. N., Kenseth, C. M., Ward, R. X., Pye, H. O. T., and Seinfeld, J. H.: An Updated Modeling Framework to Simulate Los Angeles Air Quality. Part 1: Model Development, Evaluation, and Source Apportionment, EGUsphere, 2023, 1-27, 10.5194/egusphere-2023-749, 2023.

Perdigones, B. C., Lee, S., Cohen, R. C., Park, J.-H., and Min, K.-E.: Two Decades of Changes in Summertime Ozone Production in California's South Coast Air Basin, Environmental Science & Technology, 56, 10586-10595, 10.1021/acs.est.2c01026, 2022.

Pfannerstill, E. Y., Arata, C., Zhu, Q., Schulze, B. C., Woods, R., Harkins, C., Schwantes, R. H., McDonald, B. C., Seinfeld, J. H., Bucholtz, A., Cohen, R. C., and Goldstein, A. H.: Comparison between Spatially Resolved Airborne Flux Measurements and Emission Inventories of Volatile Organic Compounds in Los Angeles, Environmental Science & Technology, 57, 15533-15545, 10.1021/acs.est.3c03162, 2023.

Pollack, I. B., Ryerson, T. B., Trainer, M., Neuman, J. A., Roberts, J. M., and Parrish, D. D.: Trends in ozone, its precursors, and related secondary oxidation products in Los Angeles, California: A synthesis of measurements from 1960 to 2010, Journal of Geophysical Research: Atmospheres, 118, 5893-5911, https://doi.org/10.1002/jgrd.50472, 2013.

Pollack, I. B., Ryerson, T. B., Trainer, M., Parrish, D. D., Andrews, A. E., Atlas, E. L., Blake, D. R., Brown, S. S., Commane, R., Daube, B. C., de Gouw, J. A., Dubé, W. P., Flynn, J., Frost, G. J., Gilman, J. B., Grossberg, N., Holloway, J. S., Kofler, J., Kort, E. A., Kuster, W. C., Lang, P. M., Lefer, B., Lueb, R. A., Neuman, J. A., Nowak, J. B., Novelli, P. C., Peischl, J., Perring, A. E., Roberts, J. M., Santoni, G., Schwarz, J. P., Spackman, J. R., Wagner, N. L., Warneke, C., Washenfelder, R. A., Wofsy, S. C., and Xiang, B.: Airborne and ground-based observations of a weekend effect in ozone, precursors, and oxidation products in the California South Coast Air Basin, Journal of Geophysical Research: Atmospheres, 117, https://doi.org/10.1029/2011JD016772, 2012.

Pusede, S. E. and Cohen, R. C.: On the observed response of ozone to NO_x and VOC reactivity reductions in San Joaquin Valley California 1995–present, Atmos. Chem. Phys., 12, 8323-8339, 10.5194/acp-12-8323-2012, 2012.

Qin, M., Murphy, B. N., Isaacs, K. K., McDonald, B. C., Lu, Q., McKeen, S. A., Koval, L., Robinson, A. L., Efstathiou, C., Allen, C., and Pye, H. O. T.: Criteria pollutant impacts of volatile chemical products informed by near-field modelling, Nature Sustainability, 4, 129-137, 10.1038/s41893-020-00614-1, 2021.

Rivellini, L.-H., Jorga, S., Wang, Y., Lee, A. K. Y., Murphy, J. G., Chan, A. W., and Abbatt, J. P. D.: Sources of Wintertime Atmospheric Organic Pollutants in a Large Canadian City: Insights from Particle and Gas Phase Measurements, ACS ES&T Air, 10.1021/acsestair.4c00039, 2024.

Robinson, A. L., Subramanian, R., Donahue, N. M., Bernardo-Bricker, A., and Rogge, W. F.: Source Apportionment of Molecular Markers and Organic Aerosol. 3. Food Cooking Emissions, Environmental Science & Technology, 40, 7820-7827, 10.1021/es060781p, 2006.

Robinson, E. S., Gu, P., Ye, Q., Li, H. Z., Shah, R. U., Apte, J. S., Robinson, A. L., and Presto, A. A.: Restaurant Impacts on Outdoor Air Quality: Elevated Organic Aerosol Mass from Restaurant Cooking with Neighborhood-Scale Plume Extents, Environmental Science & Technology, 52, 9285-9294, 10.1021/acs.est.8b02654, 2018.

Robinson, M. A., Neuman, J. A., Huey, L. G., Roberts, J. M., Brown, S. S., and Veres, P. R.: Temperature-dependent sensitivity of iodide chemical ionization mass spectrometers, Atmos. Meas. Tech., 15, 4295-4305, 10.5194/amt-15-4295-2022, 2022.

Robinson, M. A., Decker, Z. C. J., Barsanti, K. C., Coggon, M. M., Flocke, F. M., Franchin, A., Fredrickson, C. D., Gilman, J. B., Gkatzelis, G. I., Holmes, C. D., Lamplugh, A., Lavi, A., Middlebrook, A. M., Montzka, D. M., Palm, B. B., Peischl, J., Pierce, B., Schwantes, R. H., Sekimoto, K., Selimovic, V., Tyndall, G. S., Thornton, J. A., Van Rooy, P., Warneke, C., Weinheimer, A. J., and Brown, S. S.: Variability and Time of Day Dependence of Ozone Photochemistry in Western Wildfire Plumes, Environmental Science & Technology, 55, 10280-10290, 10.1021/acs.est.1c01963, 2021.

Rollins, A. W., Rickly, P. S., Gao, R. S., Ryerson, T. B., Brown, S. S., Peischl, J., and Bourgeois, I.: Single-photon laser-induced fluorescence detection of nitric oxide at sub-parts-per-trillion mixing ratios, Atmos. Meas. Tech., 13, 2425-2439, 10.5194/amt-13-2425-2020, 2020.

Ryerson, T. B., Andrews, A. E., Angevine, W. M., Bates, T. S., Brock, C. A., Cairns, B., Cohen, R. C., Cooper, O. R., de Gouw, J. A., Fehsenfeld, F. C., Ferrare, R. A., Fischer, M. L., Flagan, R. C., Goldstein, A. H., Hair, J. W., Hardesty, R. M., Hostetler, C. A., Jimenez, J. L., Langford, A. O., McCauley, E., McKeen, S. A., Molina, L. T., Nenes, A., Oltmans, S. J., Parrish, D. D., Pederson, J. R., Pierce, R. B., Prather, K., Quinn, P. K., Seinfeld, J. H., Senff, C. J., Sorooshian, A., Stutz, J., Surratt, J. D., Trainer, M., Volkamer, R., Williams, E. J., and Wofsy, S. C.: The 2010 California Research at the Nexus of Air Quality and Climate Change (CalNex) field study, Journal of Geophysical Research: Atmospheres, 118, 5830-5866, https://doi.org/10.1002/jgrd.50331, 2013.

Sakamoto, Y., Sadanaga, Y., Li, J., Matsuoka, K., Takemura, M., Fujii, T., Nakagawa, M., Kohno, N., Nakashima, Y., Sato, K., Nakayama, T., Kato, S., Takami, A., Yoshino, A., Murano, K., and Kajii, Y.: Relative and Absolute Sensitivity Analysis on Ozone Production in Tsukuba, a City in Japan, Environ Sci Technol, 53, 13629-13635, 10.1021/acs.est.9b03542, 2019.

Schauer, J. J., Kleeman, M. J., Cass, G. R., and Simoneit, B. R. T.: Measurement of Emissions from Air Pollution Sources. 1. C1 through C29 Organic Compounds from Meat Charbroiling, Environmental Science & Technology, 33, 1566-1577, 10.1021/es980076j, 1999.

Schlaerth, H. L., Silva, S. J., and Li, Y.: Characterizing Ozone Sensitivity to Urban Greening in Los Angeles Under Current Day and Future Anthropogenic Emissions Scenarios, Journal of Geophysical Research: Atmospheres, 128, e2023JD039199, https://doi.org/10.1029/2023JD039199, 2023.

Schroeder, J. R., Cai, C., Xu, J., Ridley, D., Lu, J., Bui, N., Yan, F., and Avise, J.: Changing ozone sensitivity in the South Coast Air Basin during the COVID-19 period, Atmos. Chem. Phys., 22, 12985-13000, 10.5194/acp-22-12985-2022, 2022.

Schroeder, J. R., Crawford, J. H., Fried, A., Walega, J., Weinheimer, A., Wisthaler, A., Müller, M., Mikoviny, T., Chen, G., Shook, M., Blake, D. R., and Tonnesen, G. S.: New insights into the column CH2O/NO2 ratio as an indicator of near-surface ozone sensitivity, Journal of Geophysical Research: Atmospheres, 122, 8885-8907, https://doi.org/10.1002/2017JD026781, 2017.

Seinfeld, J. H.: Urban Air Pollution: State of the Science, Science, 243, 745-752, doi:10.1126/science.243.4892.745, 1989.

Seltzer, K. M., Murphy, B. N., Pennington, E. A., Allen, C., Talgo, K., and Pye, H. O. T.: Volatile Chemical Product Enhancements to Criteria Pollutants in the United States, Environmental Science & Technology, 56, 6905-6913, 10.1021/acs.est.1c04298, 2022.

Sillman, S.: The use of NO y , H2O2, and HNO3 as indicators for ozone-NO x -hydrocarbon sensitivity in urban locations, Journal of Geophysical Research: Atmospheres, 100, 14175-14188, https://doi.org/10.1029/94JD02953, 1995.

Silvern, R. F., Jacob, D. J., Mickley, L. J., Sulprizio, M. P., Travis, K. R., Marais, E. A., Cohen, R. C., Laughner, J. L., Choi, S., Joiner, J., and Lamsal, L. N.: Using satellite observations of tropospheric NO2 columns to infer long-term trends in US NOx

https://doi.org/10.5194/egusphere-2024-1899
Preprint. Discussion started: 15 July 2024

emissions: the importance of accounting for the free tropospheric NO2 background, Atmos. Chem. Phys., 19, 8863-8878, 10.5194/acp-19-8863-2019, 2019.

Stohl, A., Forster, C., Frank, A., Seibert, P., and Wotawa, G.: Technical note: The Lagrangian particle dispersion model FLEXPART version 6.2, Atmos. Chem. Phys., 5, 2461-2474, 10.5194/acp-5-2461-2005, 2005.

Strobach, E. J., Baidar, S., Carroll, B. J., Brown, S. S., Zuraski, K., Coggon, M., Stockwell, C. E., Xu, L., Pichugina, Y. L., Brewer, A., Warneke, C., Peischl, J., Gilman, J., McCarty, B., Holloway, M., and Marchbanks, R.: An Air Quality and Boundary Layer Dynamics Analysis of the Los Angeles Basin Area During the Southwest Urban NOx and VOCs Experiment (SUNVEx), EGUsphere, 2024, 1-38, 10.5194/egusphere-2024-447, 2024.

Van Rooy, P., Tasnia, A., Barletta, B., Buenconsejo, R., Crounse, J. D., Kenseth, C. M., Meinardi, S., Murphy, S., Parker, H., Schulze, B., Seinfeld, J. H., Wennberg, P. O., Blake, D. R., and Barsanti, K. C.: Observations of Volatile Organic Compounds in the Los Angeles Basin during COVID-19, ACS Earth and Space Chemistry, 5, 3045-3055, 10.1021/acsearthspacechem.1c00248, 2021.

Venecek, M. A., Carter, W. P. L., and Kleeman, M. J.: Updating the SAPRC Maximum Incremental Reactivity (MIR) scale for the United States from 1988 to 2010, Journal of the Air & Waste Management Association, 68, 1301-1316, 10.1080/10962247.2018.1498410, 2018.

Vermeuel, M. P., Novak, G. A., Alwe, H. D., Hughes, D. D., Kaleel, R., Dickens, A. F., Kenski, D., Czarnetzki, A. C., Stone, E. A., Stanier, C. O., Pierce, R. B., Millet, D. B., and Bertram, T. H.: Sensitivity of Ozone Production to NOx and VOC Along the Lake Michigan Coastline, Journal of Geophysical Research: Atmospheres, 124, 10989-11006, https://doi.org/10.1029/2019JD030842, 2019.

Verreyken, B., Brioude, J., and Evan, S.: Development of turbulent scheme in the FLEXPART-AROME v1.2.1 Lagrangian particle dispersion model, Geosci. Model Dev., 12, 4245-4259, 10.5194/gmd-12-4245-2019, 2019.

Verreyken, B. W. D., Harkins, C., Li, M., Angevine, W., Stockwell, C., Xu, L., Coggon, M., Gilman, J., Warneke, C., Strobach, E. J., Brown, S., McCarty, B., Marchbanks, R., Baidar, S., Brewer, A., Pfannerstill, E., Arata, C., Goldstein, A., Brioude, J., and McDonald, B. C.: Top-down Evaluation of Volatile Chemical Product Emissions using a Largangian Framework, in prep., 2024.

Wagner, N. L., Riedel, T. P., Roberts, J. M., Thornton, J. A., Angevine, W. M., Williams, E. J., Lerner, B. M., Vlasenko, A., Li, S. M., Dubé, W. P., Coffman, D. J., Bon, D. M., de Gouw, J. A., Kuster, W. C., Gilman, J. B., and Brown, S. S.: The sea breeze/land breeze circulation in Los Angeles and its influence on nitryl chloride production in this region, Journal of Geophysical Research: Atmospheres, 117, https://doi.org/10.1029/2012JD017810, 2012.

Warneke, C., de Gouw, J. A., Holloway, J. S., Peischl, J., Ryerson, T. B., Atlas, E., Blake, D., Trainer, M., and Parrish, D. D.: Multiyear trends in volatile organic compounds in Los Angeles, California: Five decades of decreasing emissions, Journal of Geophysical Research: Atmospheres, 117, https://doi.org/10.1029/2012JD017899, 2012.

Warneke, C., de Gouw, J. A., Del Negro, L., Brioude, J., McKeen, S., Stark, H., Kuster, W. C., Goldan, P. D., Trainer, M., Fehsenfeld, F. C., Wiedinmyer, C., Guenther, A. B., Hansel, A., Wisthaler, A., Atlas, E., Holloway, J. S., Ryerson, T. B., Peischl, J., Huey, L. G., and Hanks, A. T. C.: Biogenic emission measurement and inventories determination of biogenic emissions in the eastern United States and Texas and comparison with biogenic emission inventories, Journal of Geophysical Research: Atmospheres, 115, https://doi.org/10.1029/2009JD012445, 2010.

Washenfelder, R. A., Young, C. J., Brown, S. S., Angevine, W. M., Atlas, E. L., Blake, D. R., Bon, D. M., Cubison, M. J., de Gouw, J. A., Dusanter, S., Flynn, J., Gilman, J. B., Graus, M., Griffith, S., Grossberg, N., Hayes, P. L., Jimenez, J. L., Kuster, W. C., Lefer, B. L., Pollack, I. B., Ryerson, T. B., Stark, H., Stevens, P. S., and Trainer, M. K.: The glyoxal budget and its contribution to organic aerosol for Los Angeles, California, during CalNex 2010, Journal of Geophysical Research: Atmospheres, 116, 10.1029/2011jd016314, 2011.

Wernis, R. A., Kreisberg, N. M., Weber, R. J., Drozd, G. T., and Goldstein, A. H.: Source apportionment of VOCs, IVOCs and SVOCs by positive matrix factorization in suburban Livermore, California, Atmos. Chem. Phys., 22, 14987-15019, 10.5194/acp-22-14987-2022, 2022.

Wild, R. J., Edwards, P. M., Dubé, W. P., Baumann, K., Edgerton, E. S., Quinn, P. K., Roberts, J. M., Rollins, A. W., Veres, P. R., Warneke, C., Williams, E. J., Yuan, B., and Brown, S. S.: A Measurement of Total Reactive Nitrogen, NOy, together with NO2, NO, and O3 via Cavity Ring-down Spectroscopy, Environmental Science & Technology, 48, 9609-9615, 10.1021/es501896w, 2014.

Wolfe, G. M., Marvin, M. R., Roberts, S. J., Travis, K. R., and Liao, J.: The Framework for 0-D Atmospheric Modeling (F0AM) v3.1, Geosci. Model Dev., 9, 3309-3319, 10.5194/gmd-9-3309-2016, 2016.

Wu, S., Lee, H. J., Anderson, A., Liu, S., Kuwayama, T., Seinfeld, J. H., and Kleeman, M. J.: Direct measurements of ozone response to emissions perturbations in California, Atmos. Chem. Phys., 22, 4929-4949, 10.5194/acp-22-4929-2022, 2022.

Wu, S., Alaimo, C. P., Zhao, Y., Green, P. G., Young, T. M., Liu, S., Kuwayama, T., Coggon, M. M., Stockwell, C. E., Xu, L., Warneke, C., Gilman, J. B., Robinson, M. A., Veres, P. R., Neuman, J. A., and Kleeman, M. J.: O3 Sensitivity to NOx and VOC During RECAP-CA: Implication for Emissions Control Strategies, ACS ES&T Air, 10.1021/acsestair.4c00026, 2024.

Yu, K. A., Li, M., Harkins, C., He, J., Zhu, Q., Verreyken, B., Schwantes, R. H., Cohen, R. C., McDonald, B. C., and Harley, R. A.: Improved Spatial Resolution in Modeling of Nitrogen Oxide Concentrations in the Los Angeles Basin, Environmental Science & Technology, 57, 20689-20698, 10.1021/acs.est.3c06158, 2023.

Yuan, B., Koss, A. R., Warneke, C., Coggon, M., Sekimoto, K., and de Gouw, J. A.: Proton-Transfer-Reaction Mass Spectrometry: Applications in Atmospheric Sciences, Chemical Reviews, 117, 13187-13229, 10.1021/acs.chemrev.7b00325, 2017.

Zare, A., Romer, P. S., Nguyen, T., Keutsch, F. N., Skog, K., and Cohen, R. C.: A comprehensive organic nitrate chemistry: insights into the lifetime of atmospheric organic nitrates, Atmos. Chem. Phys., 18, 15419-15436, 10.5194/acp-18-15419-2018, 2018.

Zhu, Q., Schwantes, R. H., Coggon, M., Harkins, C., Schnell, J., He, J., Pye, H. O. T., Li, M., Baker, B., Moon, Z., Ahmadov, R., Pfannerstill, E. Y., Place, B., Wooldridge, P., Schulze, B. C., Arata, C., Bucholtz, A., Seinfeld, J. H., Warneke, C., Stockwell, C. E., Xu, L., Zuraski, K., Robinson, M. A., Neuman, J. A., Veres, P. R., Peischl, J., Brown, S. S., Goldstein, A. H., Cohen, R. C., and McDonald, B. C.: A better representation of volatile organic compound chemistry in WRF-Chem and its impact on ozone over Los Angeles, Atmos. Chem. Phys., 24, 5265-5286, 10.5194/acp-24-5265-2024, 2024a.

Zhu, Q., Schwantes, R. H., Stockwell, C. E., Harkins, C., Lyu, C., Coggon, M., Warneke, C., Schnell, J., He, J., Pye, H. O. T., Li, M., Ahmadov, R., Pfannerstill, E. Y., Place, B., Wooldridge, P., Schulze, B. C., Arata, C., Bucholtz, A., Seinfeld, J. H., Xu, L., Zuraski, K., Robinson, M. A., Neuman, J. A., Gilman, J., Lamplugh, A., Veres, P. R., Peischl, J., Rollins, A., Brown, S. S., Goldstein, A. H., Cohen, R. C., and McDonald, B. C.: Co-benefits of the Zero-Emission Vehicle Adoption on CO2

Emissions and O3 Pollution in Los Angeles, in prep., 2024b.